RECEIVED
LAWRENCE
RADIATION LABORATORY

JUN 13 1974

LIBRARY AND
DOCUMENTS SECTION

LBL-2715
C. 2

UNTEMPERED ULTRA HIGH STRENGTH STEELS OF HIGH FRACTURE TOUGHNESS

E. R. Parker, V. F. Zackay, G. Y. Lai and R. M. Horn

April 1974

Prepared for the U. S. Atomic Energy Commission
under Contract W-7405-ENG-48
and
AMMRC Contract No. DAAG46-73-C-0120

TWO-WEEK LOAN COPY

This is a Library Circulating Copy which may be borrowed for two weeks. For a personal retention copy, call Tech. Info. Division, Ext. 5545

LAWRENCE BERKELEY LABORATORY
UNIVERSITY OF CALIFORNIA
BERKELEY

LBL-2715
C. 2

DISCLAIMER

This document was prepared as an account of work sponsored by the United States Government. While this document is believed to contain correct information, neither the United States Government nor any agency thereof, nor the Regents of the University of California, nor any of their employees, makes any warranty, express or implied, or assumes any legal responsibility for the accuracy, completeness, or usefulness of any information, apparatus, product, or process disclosed, or represents that its use would not infringe privately owned rights. Reference herein to any specific commercial product, process, or service by its trade name, trademark, manufacturer, or otherwise, does not necessarily constitute or imply its endorsement, recommendation, or favoring by the United States Government or any agency thereof, or the Regents of the University of California. The views and opinions of authors expressed herein do not necessarily state or reflect those of the United States Government or any agency thereof or the Regents of the University of California.

Contents

I. Introduction 1

II. Microstructural Features Influencing Fracture Toughness of AISI 4340 Steel 3

A. Experimental Procedure 3

B. Experimental Results 4

1. Mechanical Properties 4

2. Fracture Morphology 5

3. Microstructure of As-Quenched AISI 4340 Steel 6

a. Martensite Morphology 6

b. Substructure of Martensite 7

c. Retained Austenite 8

d. Autotempering 9

4. Structure of Tempered Martensite 10

C. Discussion 10

1. Factors contributing to the Improvement of Fracture Toughness of As-Quenched AISI 4340 Steel 10

2. Tempered Martensite Embrittlement 12

III. Microstructure, Fracture Toughness and Fatigue Crack Growth of 5 Mo-0.3 C Steel 17

A. Experimental Procedure 17

B. Results and Discussion 18

1. Influence of Tempering Temperature on Strength and Toughness

2. Effect of Microstructural Features on Crack Propagation . . 19

3. Microstructure and Crack Growth Rates of the As-Quenched Steel 19

4. Microstructure and Fatigue Crack Growth Rates After Tempering at 225°C 21

5. Microstructure and Fatigue Crack Growth Rates After Tempering at 300°C 22

6. Microstructure and Fatigue Crack Growth After Tempering at 500°C 23

7. Microstructure and Fatigue Crack Growth After Tempering at 600°C 24

IV. Summary and Conclusions 26

Acknowledgements 28

References 29

Table 32

Figure Captions 33

Figures 38

UNTEMPERED ULTRA HIGH STRENGTH STEELS OF HIGH FRACTURE TOUGHNESS

E. R. Parker, V. F. Zackay, G. Y. Lai and R. M. Horn

Inorganic Materials Research Division, Lawrence Berkeley Laboratory and
Department of Materials Science and Engineering, College of Engineering;
University of California, Berkeley, California 94720

ABSTRACT

The objective of the present investigation was to establish, in high yield strength steels, relationships between microstructure, fracture toughness and fatigue crack growth. Extensive microstructural examination and characterization were conducted on as-quenched, and quenched and tempered AISI 4340 steel which was austenitized both at the conventional (870°C) and the high (1200°C) austenitizing temperatures. Changes in fracture toughness resulting from variations in austenitizing and tempering treatments were related to changes in the amount and distribution of retained austenite, the morphology and distribution of carbides, and the martensite substructure and morphology. The influence of microstructure on fatigue crack propagation was investigated in as-quenched, and quenched and tempered 5Mo-0.3C secondary hardening steel. Microstructures resulting from several different tempering treatments were characterized and attempts were made to relate microstructural changes to observed differences in strength, fracture toughness and fatigue crack growth behavior.

I. INTRODUCTION

A large number of currently available high yield strength steels are limited by their low toughness, especially at yield strength levels exceeding 200,000 psi. At such high yield strength levels catastrophic failure can occur at very low critical flaw sizes. It is now well known that microstructure plays an important role on the fracture toughness of high yield strength steels when they are subjected to monotonic loading. The influence of microstructure on crack growth under cyclic loading, on the other hand, is a subject where a great deal of controversy still exists.

An essential first step in understanding the role of microstructure on fracture toughness or fatigue crack growth is characterization of microstructural features. A combination of optical, electron and X-ray metallography and scanning electron fractography in conjunction with mechanical testing is needed for microstructural characterization. When microstructural features that result in low toughness are identified, it should be possible to eliminate or minimize such undesirable features by changing either the alloy composition, or the heat treating procedure, or both. The main objective of the present study was to establish, using high yield strength steels, relationships between microstructure and fracture toughness on one hand, and microstructure and fatigue crack growth on the other.

The low alloy AISI 4340 steel was chosen for obtaining relationships between microstructure and toughness. The conventional heat treatment used for this steel consists of austenitizing at the lower end of the austenite phase region (870°C) to minimize grain size, following which

the steel is oil quenched and then tempered. Recently it was shown (1) that the room temperature plane strain fracture toughness of as-quenched AISI 4340 steel was considerably improved when, instead of using the conventional austenitizing treatment, the steel was first austenitized for one hour at 1200°C, then furnace cooled to 870°C, held for 30 min, and oil quenched. In the present investigation extensive microstructural examination and characterization were conducted on AISI 4340 steel which was austenitized both by the 870°C and the 1200°C→870°C treatments, and tempered at several temperatures. The increase in fracture toughness resulting from the use of high austenitizing temperature was related to several microstructural features. The morphology and distribution of carbides that precipitated during tempering were also examined and possible reasons were extended for the observed influence of tempering temperature on fracture toughness.

Microstructural influences on fatigue crack propagation were investigated in a 5 Mo-0.3 C secondary hardening steel. Earlier studies (2) had shown that large variations in toughness at equivalent yield strengths occurred in quenched and tempered 5 Mo-0.3 C steel. Microstructural changes resulting from different tempering treatments were characterized by transmission electron microscopy and used to explain the observed variation in fracture toughness. Fatigue crack growth rates were measured for several stress intensity ranges. Plots of $\frac{da}{dN}$ (change in crack length per cycle of loading) and ΔK (stress intensity range applied during cyclic loading) were obtained for the 5 Mo-0.3 C steel tested in as-quenched and several quenched and tempered conditions. Attempts were made to relate microstructure, fatigue crack growth rates, fracture toughness and strength.

II. MICROSTRUCTURAL FEATURES INFLUENCING FRACTURE TOUGHNESS OF AISI 4340 STEEL

A. EXPERIMENTAL PROCEDURE

The AISI 4340 steel used in this investigation was received in a fully annealed condition. It had the following chemical composition in weight percent: 0.40 carbon, 0.80 manganese, 0.72 chromium, 1.65 nickel, 0.24 molybdenum, 0.24 silicon, 0.19 copper, 0.01 sulphur and 0.004 phosphorus. Two austenitizing treatments were used throughout this investigation. One was the conventional heat treatment which consisted of austenitizing at 870°C for one hour and oil quenching. The second treatment consisted of austenitizing at 1200°C for one hour followed by cooling to 870°C and holding for 30 min prior to oil quenching. Tempering was carried out for one hour at various temperatures. Austenitizing treatments were conducted in an argon atmosphere, and salt baths were used for tempering.

Tensile properties were measured with round specimens of 0.357 in. diameter and 1.4 in. gauge length, and with threaded ends. These specimens were ground from the blanks that had been previously heat treated. The plane strain fracture toughness was determined using the ASTM specified compact tension testing specimens (3). All fracture toughness specimens were machined from 5/8 in. thick plates to final dimensions except for the thickness and the 0.008 in. crack starter slot. After heat treating 0.010 in. was ground off each surface and the 0.008 in. thick slot was machined. A 300,000 lb MTS machine was used for tensile testing, fatigue precracking of the compact tension specimen, and for fracture toughness testing. Both tensile and fracture toughness tests were performed at room

temperature at a cross head speed of 0.04 in./min; all specimens were tested in the longitudinal direction. The stress intensities were determined from the collocation solution given by Srawley and Gross (4).

Thin foils for transmission electron microscopy were obtained directly from the fracture toughness specimens to insure that there would be no ambiguity in correlating microstructure with fracture toughness. Foil preparation consisted of chemically thinning the 0.020 in. thick samples, which were mechanically sectioned in flood cooling with extreme care from fracture toughness specimens, in a mixture of hydrofluoric acid and hydrogen peroxide, down to a thickness of 0.005 in. followed by electropolishing in chromic-acetic acid electrolyte, using the window technique. Foils were examined in a Siemens Elmiskop IA transmission electron microscope operated at 100 kV.

The fracture surfaces of fracture toughness specimens were examined in a JEOLCO JSM-U3 scanning electron microscope with a secondary emission operated at 25 kV.

B. EXPERIMENTAL RESULTS

1. Mechanical Properties

The room temperature yield (0.2 pct offset) and ultimate tensile strengths and the plane strain fracture toughness (K_{IC}) of AISI 4340 steel are plotted in Fig. 1 as a function of tempering temperature for both the 870°C and the 1200°C→870°C austenitizing treatments. From the figure it is evident that the yield and tensile strengths in the as-quenched condition were essentially the same for the two austenitizing treatments. Also, the variation of strength with increase in tempering temperature up to 350°C was similar for the two austenitizing treatments.

However, a remarkable inprovement in plane strain fracture toughness was observed for the as quenched steel when the austenitizing temperature was raised to 1200°C.

The influence of tempering temperature on plane strain fracture toughness was significantly different for the two austenitizing treatments. Considerable improvement in toughness was observed when the steel austenitized at 870°C was tempered at 200°C. The steel austenitized at 1200°C exhibited a smaller increase in toughness when tempered at the same temperature. When the tempering temperature was raised to 280°C, there was little change in toughness for the 870°C austenitizing treatment while the steel tempered following the 1200°C→870°C treatment exhibited a considerable decrease in toughness. The toughness of the 1200°C austenitized steel did not appreciably change when the tempering temperature was raised to 350°C. The steel austenitized at 870°C, however, showed a further increase in toughness. The toughness of the steel austenitized at 870°C for quenched and tempered conditions, was in general agreement with published data (5,6).

2. Fracture Morphology

Scanning electron microscope examination of broken plane strain fracture toughness specimens indicated that the mode of fracture for the as-quenched specimens changed from a mixture of dimpled rupture and quasi-cleavage to predominantly dimpled rupture when austenitizing temperature was raised from 870°C to 1200°C, Fig. 2.

The fracture surface of specimen austenitized at 870°C and tempered at 280°C (Fig. 3(a)) exhibited dimples and quasi-cleavage facets, and the fracture was similar in appearance to that of the as-quenched specimen

with the same austenitizing treatment, except that more dimples and tear ridges were noted in the tempered specimen. The fracture surface of the specimen austenitized at 1200°C and tempered at 200°C was similar to that of the as-quenched specimen except that deeper dimples, indicating more plastic deformation, were observed in the tempered specimen. Intergranular fracture at prior austenite grain boundaries was observed in specimens tempered at 280 and 350°C following austenitizing at 1200°C, Fig. 3(b).

3. Microstructure of As-Quenched AISI 4340 Steel

a. Martensite Morphology. The increase in austenitizing temperature from 870°C to 1200°C resulted in an increase in grain size from ASTM 7-8 to ASTM 0-1. Extensive examination by optical and transmission electron microscopy indicated that oil quenching from both austenitizing temperatures resulted in a predominantly martensitic microstructure with a small amount of lower bainite. No upper bainite or proeutectoid ferrite was detected in as-quenched steels.

Two types of martensite morphology were observed in the as-quenched steel austenitized both at 870°C and 1200°C. The first type, often referred to as plate martensite (7), consisted of large martensite plates, which formed as individual plates (rather than in groups), and some are marked P in Fig. 4(a), (b) and (c). The second type of martensite was lath martensite (7-9) in which laths were generally aligned parallel to one another in groups or packets, Fig. 4(b), (c) and (d). The plate martensite in the steel austenitized at 870°C generally extended across an entire austenite grain, Fig. 4(b), while in the steel austenitized at 1200°C the martensite plates nucleated at prior austenite grain boundaries

were arrested in the grain interior, Fig. 4(c).

b. Substructure of Martensite. The size of martensite laths did not differ significantly by the change in austenitizing temperature, Fig. 4(b) and (d). The martensite laths within a packet were generally separated from one another by low angle boundaries, and contained a high density of tangled dislocations. Occasionally, the laths contained internal twins, Fig. 4(b) and (d). However, the amount of these twins was small and approximately the same for both the 870°C and the 1200°C → 870°C austenitizing treatments.

The large martensite plates observed in the steel austenitized at 870°C consisted of two different types of substructure. Some plates were highly dislocated (Fig. 4(b)) while many others contained extensive and fine transformation twins in addition to dislocations, Fig. 5. Appropriate foil tilting insured that the observed absence of twinning in some plates was real and was not caused by the orientation of the plate with respect to the electron beams. Furthermore, it was found that the untwinned plates contained numerous fine carbides that resulted from autotempering whereas the twinned plates did not. This suggested that the twinned plates were formed at lower temperatures where carbide formation did not occur. The twins in martensite plates were identified by selected area diffraction analysis and dark field imaging of twin spots, and their twin planes were determined as $\{112\}_M$, Fig. 6. The extensively twinned martensite plates were eliminated when the steel was austenitized at 1200°C. The large martensite plates observed in the steel oil quenched following the 1200°C→870°C treatment contained numerous fine cross-hatched ε carbides which formed as a result of autotempering.

There was a definite lack of twinning, Fig. 7. The cross-hatched arrangement of ε carbides was similar to that observed by other investigators (10). The occurrence of autotempering in the as-quenched specimens is discussed later.

c. Retained Austenite. Another prominent change in microstructure when austenitizing temperature was raised from 870°C to 1200°C was the considerable increase in the amount of retained austenite. The specimen austenitized at 870°C and oil quenched contained very little retained austenite, as indicated by an examination of the bright field micrograph in Fig. 8(a) and the dark field micrograph (obtained from an austenite reflection) in Fig. 8(b). Conversely, the 1200°C→870°C treatment resulted in extensive retained austenite films around martensite laths as shown by the bright field micrograph in Fig. 9(a) and the dark field micrograph in Fig. 9(b). The dark field image in Fig. 9(b) was obtained from an (002) austenite reflection in the diffraction pattern shown in Fig. 9(c). The diffraction pattern shown in Fig. 9(c) is indexed in Fig. 9(d).

The retained austenite, approximately 100 to 200Å thick, exhibited the Kurdjumov-Sachs orientation relationship with respect to martensite, i.e., $\langle 110 \rangle_\gamma \parallel \langle 111 \rangle_M$, Fig. 9(c), which was in agreement with the results of earlier workers (11). Additional transmission microscopy of specimens refrigerated in liquid nitrogen immediately after quenching indicated that the retained austenite was thermally stable down to -196°C. The presence of retained austenite was not detected by X-ray methods. This could mean either that the total amount of retained austenite was within the

limit of detection by X-ray measurements (approximately within 3 pct) or that the amount of retained austenite, which may well be above the limit of detection by X-ray methods, was too highly deformed to allow detection.

d. Autotempering. The occurrence of autotempering was observed in as-quenched specimens austenitized both at 870°C and 1200°C. Two types of carbides, namely cementite and ε carbide, formed as a result of autotempering. Cementite formed as fine particles within martensite laths. A typical micrograph illustrating autotempered martensite containing cementite is shown in Fig. 10 for the 1200°C→870°C austenitizing treatment. A similar structure was also obtained for the 870°C treatment. The ε carbide that formed in a cross-hatched pattern in autotempered martensite was identified by trace analysis of its habit planes and by dark field imaging. Micrographs illustrating the morphology of ε carbide are shown in Fig. 11 for both the 1200°C→870°C and the 870°C austenitizing treatments. The present investigation showed that ε carbide formed on $\{100\}_\alpha$ planes and along $\langle 100\rangle_\alpha$ directions, in agreement with the findings of other investigators (10,12).

The distinction between autotempered martensite and untempered martensite required a simultaneous examination of both bright and dark field images, and selected area electron diffraction analysis involving extensive foil tilting. This led to great difficulty in attempts to obtain quantitative estimates of the differences in the amounts of autotempered martensite resulting from the two different austenitizing treatments.

4. Structure of Tempered Martensite

When specimens austenitized at either 870°C or 1200°C were tempered at 200°C, a uniform dispersion of ε carbides formed within martensite laths and plates. No lath boundary carbides were observed. The retained austenite in as-quenched specimens did not decompose during tempering at 200°C. However, it decomposed at 280°C and 350°C.

In specimens austenitized both at 870°C and 1200°C cementite was the predominant carbide that formed during tempering at 280°C although in a few regions ε carbide was also detected. Cementite precipitation occurred both at lath boundaries and within laths and plates as illustrated in Fig. 12. In addition the precipitation of cementite as discrete platelets at prior austenite grain boundaries was also observed as shown in Figs. 13 and 14. Grain boundary precipitation of carbides did not result in continuous carbide networks. The distribution and morphology of cementite that formed on tempering at 280°C were not significantly different for the two austenitizing treatments.

C. DISCUSSION

1. Factors Contributing to the Improvement of Fracture Toughness of As-Quenched AISI 4340 Steel

It was evident from the present investigation that a large improvement was obtained in the fracture toughness of as-quenched and low-temperature (200°C) tempered AISI 4340 steel by using a much higher austenitizing temperature (1200°C) than that conventionally used (870°C). This improvement in fracture toughness was accompanied by a change of fracture mode from a mixture of dimpled rupture and quasi-cleavage to predominantly dimpled rupture when the austenitizing temperature was changed from 870°C to 1200°C.

The as-quenched structure for both austenitizing treatments consisted of autotempered and untempered martensites. It is well known that increased autotempering causes improvement in toughness and decrease in tensile strength of as-quenched martensite. The difference, if any, in the extent of autotempering in the as-quenched structures obtained in the present investigation for the 870°C and the 1200°C→870°C austenitizing treatments could not be quantitatively estimated. However, the similar ultimate tensile strength levels in as-quenched conditions for both austenitizing treatments suggested that difference in the extent of autotempering, if any, was not large enough to contribute to the observed large difference in fracture toughness.

The martensite morphology in as-quenched structures following both austenitizing treatments was characterized by laths and plates. For both austenitizing treatments the martensite laths were dislocated and few internal twins were present within the laths. However, in the steel austenitized at 870°C a large number of martensite plates contained extensive and fine internal twins. These twinned martensite plates were virtually eliminated when the steel was austenitized at 1200°C. It was concluded that the elimination of twinned martensite plates was at least partly responsible for the observed increase in fracture toughness of specimens austenitized at 1200°C. The loss of toughness due to the presence of extensive twinning has also been reported by other investigators (13,14) who compared the toughness between twinned martensite and lower bainite (untwinned) and between twinned martensite and dislocated martensite. The exact role of twinning on toughness is not yet clear. Kelly and Nutting (11) suggested that the available number of slip systems

is reduced by a factor of four when twinning occurs since the operative slip system must be such that the slip plane and the slip direction are common to both the twin and the matrix. Krauss and Pitsch (15) and Bevis, et al. (16) indicated that martensite with internal twins is more likely to deform by mechanical twinning than by slip. Cracks induced by twins in metals have been observed by Gilbert, et al. (17).

Another prominent microstructural change accompanying the increase of austenitizing temperature from 870°C to 1200°C was a large increase in the amount of retained austenite. Austenite is known to be a tough phase which can effectively arrest cracks. Increases in toughness with increasing retained austenite content in steels have been observed before (18). It has been suggested that the distribution of retained austenite may have a greater influence on toughness than the total amount of retained austenite. The austenite observed in AISI 4340 steel austenitized at 1200°C was in the form of films surrounding martensite laths. Austenite in such form can relax stress concentration and delay the formation of microcracks, and also can effectively arrest propagation of microcracks when they do develop. This can result in considerable enhancement of fracture toughness.

2. Tempered Martensite Embrittlement

Room temperature plane strain fracture toughness measurements failed to reveal tempered martensite embrittlement in specimens austenitized at 870°C (ASTM grain size 7-8) and tempered at 200 to 350°C. The fracture mode of all tempered specimens was observed to be transgranular with respect to prior austenite grains, and was characterized by a mixture of dimpled rupture and quasi-cleavage. In contrast, specimens austenitized

at 1200°C to attain an austenite grain size of ASTM 0-1, exhibited embrittlement when they were tempered at 280°C and 350°C. The fracture of embrittled specimens was intergranular along prior austenite grain boundaries, while that of unembrittled specimens (as-quenched condition or tempered at 200°C) occurred by dimpled rupture. Microstructural observations indicated that embrittlement occurred when cementite was the predominant precipitate formed during tempering. However, the observed difference in embrittlement behavior between the two austenitizing treatment could not be attributed to cementite precipitation alone since the distribution and morphology of cementite at lath boundaries and prior austenite grain boundaries were similar for the two treatments used in the present investigation, and yet, specimens austenitized at 1200°C were embrittled on tempering while those austenitized at 870°C were not. It was believed that the difference in fracture behavior between the 1200°C austenitized (coarse grains) specimens and the 870°C austenitized (fine grains) specimens after tempering at 280°C and 350°C might be due to some other factors which are discussed below.

Tempered martensite embrittlement has been previously reported by a number of investigators (19-21) who based their conclusions on room temperature Charpy impact tests. With recent developments in fracture toughness theory and testing, considerable data have been produced on the effect of tempering temperature on fracture toughness of AISI 4340 and other steels which were austenitized at around 870°C (resulting in fine austenite grains) prior to tempering (5,6,22-25). All these data showed no evidence of tempered martensite embrittlement. In fact, some investigations showed a smooth increase in fracture toughness with increasing tempering temperature, while others showed that fracture

toughness was relatively constant in the 200°C-300°C range and increased rapidly at higher tempering temperatures. The results of the present investigation were in general agreement with earlier findings in that there was no apparent embrittlement in specimens austenitized at 870°C.

Ronald (26) recently investigated tempered martensite embrittlement of AISI 4340 by using V-notched and fatigue-precracked Charpy specimens of various sizes tested in impact and slow bend modes. The specimens were austenitized at about 850°C prior to tempering, and were tested at room temperature. In a plot of energy absorbed per unit area in breaking the specimen vs tempering temperature, he found that whether or not embrittlement could be detected was dependent on the type and size of the specimen, and also on the type of test, i.e., impact or slow bend. In impact testing, embrittlement was always observed with varied specimen thickness whether specimens were V-notched or precracked. In slow bend testing, embrittlement was always observed in V-notched specimens with varied thickness from 0.030 to 0.394 in., but when precracked specimens were used embrittlement was observed only in thin specimens from 0.030 to 0.050 in., and was not observed in thick specimens from 0.075 to 0.394 in. Kula and Anctil (6), while observing tempered martensite embrittlement of AISI 4340 in room temperature Charpy impact tests, found no evidence of embrittlement in room temperature K_{IC} tests. However, they observed a slight embrittlement when K_{IC} tests were conducted at -45°F.

The above discussion indicates that the detection of tempered martensite embrittlement depends on many factors including the type and size of test specimens, loading rate (static or dynamic loading), and testing temperature. Varying some of these parameters, for example,

increasing the loading rate from static to dynamic loading or decreasing testing temperature, could enhance the detection of tempered martensite embrittlement.

There is little information on transition temperature for fracture toughness values in low alloy high strength steels. Steigerwald (27) observed that the plane strain fracture toughness continued to decrease relatively sharply as the testing temperature was lowered from room temperature to -73°C for AISI 4340 and 4140 steels austenitized at 850°C and tempered at either 260°C or 427°C. It is well known that increasing grain size results in an increase in Charpy impact ductile to brittle transition temperature. It is reasonable to expect that increasing grain size may also result in an increase in fracture toughness transition temperature. The likelihood of detecting tempered martensite embrittlement is enhanced when the testing temperature is at or below the fracture toughness transition temperature. It was believed that the observed tempered martensite embrittlement in the 1200°C austenitized specimens of the present investigation was due to increased prior austenite grain size which possibly raised the fracture toughness transition temperature to above room temperature.

Although the mechanism of tempered martensite embrittlement cannot be determined from the results of the present investigation, some general comments can be made. Several investigators (21,28,29) have reported that the occurrence of embrittlement is associated with the precipitation of cementite platelets. It has been further demonstrated by Alstetter, et al. (30) that increased silicon content in steel raises the temperature at which cementite precipitation first occurs and also raises the tempering

temperature at which embrittlement occurs. The microstructural observations of the present investigation substantiated that embrittlement occured when cementite was the predominant carbide phase. In addition to the precipitation of cementite both within the laths and at lath boundaries, discrete precipitation of cementite platelets was observed at prior austenite grain boundaries. The fracture mode of the embrittled steel was intergranular along prior austenite grain boundaries. In a similar investigation on AISI 4130 steel which also exhibited tempered martensite embrittlement with an intergranular fracture in 1200°C austenitized specimens tempered at 280°C, discrete cementite platelets were observed at prior austenite grain boundaries (31). It was not clear whether the discrete grain boundary carbide alone, under appropriate conditions of testing temperature, loading rate, prior austenite grain size, etc., could induce intergranular fracture and cause embrittlement. Recent work by Capus and Mayer (32) has shown that the presence of certain impurity elements has a significant influence on tempered martensite embrittlement. An embrittlement model proposed by Kula and Anctil (6) suggests that when cementite at prior austenite grain boundaries grows during tempering, certain impurity elements such as phosphorus, which might be more soluble in ferrite than in cementite, will diffuse out of cementite into the surrounding ferrite. This results in a segregated film of impurities at the interface between ferrite and cementite. These impurities might lower the interfacial energy and provide a weak interface for fracture.

III. MICROSTRUCTURE, FRACTURE TOUGHNESS AND FATIGUE CRACK GROWTH OF 5 Mo-0.3 C STEEL

A. EXPERIMENTAL PROCEDURE

Three 20 lb vacuum melted ingots were used in this study. The compositions are given in Table I. Each ingot was homogenized at 1100°C for 24 hr, hot-forged at 1100°C, and then hot-rolled at 1100°C into bars of width 2 3/4 in. and thickness 5/8 in. Tensile and fracture toughness specimens were cut from the rolled bars, austenitized at 1200°C for one hour in an argon atmosphere, ice-brine quenched, and refrigerated in liquid nitrogen to obtain a fully martensitic structure. In addition to the as-quenched condition, specimens tempered at 225°C, 300°C, 500°C and 600°C were tested. The specimens requiring tempering were held for one hour at the desired temperature in a salt bath.

Compact tension fracture toughness specimens meeting ASTM specifications (3) were used for the fatigue tests. All specimens were 9/16 in. thick to insure plane strain conditions. Standard 1/4 in. round tensile specimens of one inch gage length and with threaded ends were used to measure tensile properties.

Fatigue tests were carried out at room temperature (20-25°C) in air (45-55 pct relative himidity) in a 300,000 lb capacity MTS machine. The specimens were tested at a frequency of 6 Hz under sinusoidal tension-tension cycling. Fatigue crack advancement was measured optically using a traveling microscope. Increases in crack advancement of 0.001 in. could be measured on the pre-polished specimen. The crack advancement, Δa, was measured on both surfaces of the specimen, and an average was used. The load was monitored continuously, and the tests were carried out using a

minimum to maximum load ratio of R = 0.11 (where $R = P_{min}/P_{max}$). Because the minimum and maximum loads were kept constant, the stress intensity range increased as the crack length increased. The formulation of the stress intensity for the compact tension specimen used is as follows:

$$K_I = \frac{P}{W^{1/2}B} \cdot \left[29.6\left(\frac{a}{w}\right)^{1/2} - 185.5\left(\frac{a}{w}\right)^{3/2} + 655.7\left(\frac{a}{w}\right)^{5/2} - 1017.0\left(\frac{a}{w}\right)^{7/2} + 638.9\left(\frac{a}{w}\right)^{9/2}\right]$$

Because the stress intensity range increased, many data points were collected for each specimen. Fracture toughness tests were carried out using the fatigue specimens, when $\frac{a}{w}$ reached about 0.7.

Fracture surfaces of the fatigue specimens were examined in a JEOLCO JSM-U3 scanning electron microscope. Optical metallography was performed on specimens cut from the fatigue specimens. The specimens were mechanically polished and etched with a 5 pct nital solution.

B. RESULTS AND DISCUSSION

1. Influence of Tempering Temperature on Strength and Toughness

The variations of the room temperature yield strength and plane strain fracture toughness behavior with tempering treatment, are shown in Fig. 15 and Fig. 16. For the secondary hardening steel used, there was an increase in yield strength with tempering temperature in the neighborhood of 600°C, where a peak in hardness and yield strength occurred. The fracture toughness dropped significantly where tempering temperatures greater than 225°C were used. The lowest value observed at the tempering temperature of 600°C was similar to the value shown by Goolsby (2).

2. Effect of Microstructural Features on Crack Propagation

The Paris relation (33) was used as a basis for the fatigue crack growth data, and a least-squares log-log fit (34) was used to determine the parameters in the empirical relation, as shown in Figs. 17 through 21. Duplicate tests were conducted to determine the fatigue crack growth parameters for all tempering treatments, except the 600°C treatment.

In the following discussion an attempt is made to determine how fatigue crack growth is related to the microstructural features of the steel and to establish whether the same microstructural features affecting yield strength and fracture toughness affect fatigue crack growth properties in a similar way.

3. Microstructure and Crack Growth Rates of the As-Quenched Steel

Figure 22 is an optical photomicrograph showing the martensitic structure present in the as-quenched material. The large prior austenite grain size, which is not evident from the figure, was 300-400μ. As shown by transmission electron microscopy in Fig. 23, extensive autotempering was present in the martensite laths. Extensive autotempering occurred because the M_s temperature was high (about 425°C). The high M_s of the material was a consequence of the relatively low carbon content (0.3 pct) and the high austenitizing temperature. Goolsby has shown, using dark field transmission electron microscopy techniques, that the only carbide present in the autotempered martensite was comentite (2). No ε carbide was detected. The martensite was predominantly the dislocated lath type, which is characteristic of steels of this carbon content (11). Internal twinning was observed only in isolated regions.

Figure 24 is a composite scanning electron micrograph of the fatigue fracture. The ΔK level in the area shown was 35 ksi-in.$^{1/2}$. The macroscopically measured crack growth rate at this ΔK was 1.5×10^{-5} in./cycle. Features characteristic of quasi-cleavage were observed throughout the fatigue area. An example of this is shown in the fatigue area in Fig. 24 at point A. This quasi-cleavage feature may account for the scatter in some of the data. Surrounding the quasi-cleavage area, A in Fig. 24, is evidence of localized plastic instability (at B) on the fatigue fracture surface. The diffuse markings resembling striations (at B) also suggest that the fatigue crack was not confined to a single plane. At C in Fig. 24, indications of striations are also seen. Striations are revealed more clearly at A in Fig. 25, which is a scanning electron micrograph of another area where the ΔK was 40 ksi-in.$^{1/2}$. The measured average microscopic spacing of these striations (1.6×10^{-5} in.) was approximately equal to the macroscopically measured crack growth rate (1.8×10^{-5} in./cycle). The fatigue crack growth rate followed an approximate second power dependence ($m = 2.05$). Growth properties were associated with a microstructure characterized by autotempered laths of predominantly dislocated martensite. The observed scatter in the crack growth rate data was ascribed to certain unidentified embrittling microstructural features, the presence of which was revealed by quasi-cleavage areas, as shown in Fig. 24.

The excellent strength and fracture toughness properties of the steel in the as-quenched condition were attributed to the relatively uniform microstructure, characterized by dislocated autotempered martensite. No residual carbides or extensive lath boundary precipitation products were

observed in transmission electron microscopy studies. The yield strength of the as-quenched material was over 200,000 psi and the fracture toughness was about 90 ksi-in.$^{1/2}$.

Figure 26 shows the fatigue crack propagation rates of the as-quenched 5 Mo-0.3 C steel along with crack growth rates for martensitic steels having yield strengths of about 200,000 psi (35-38). As the figure shows, the as-quenched 5 Mo-0.3 C steel displayed fatigue crack propagation rates at high values of ΔK that were appreciably less than those reported for other steels.

4. Microstructure and Fatigue Crack Growth Rates After Tempering at 225°C

Tempering at 225°C resulted in a significant increase in fracture toughness, as shown in Fig. 16, and a drop in yield strength, which was shown in Fig. 15. Transmission electron microscopy revealed that tempering at 225°C led to no obvious alteration in the microstructure from that in the as-quenched condition (2), although the lower yield strength reflected normal tempering effects, such as additional precipitation and growth of carbide particles.

The fatigue crack growth rates in the tempered samples were also characterized by a second power dependence (1.9); the growth rates for a given ΔK were essentially the same as those for the as-quenched specimens. The appearance of the fatigue fracture surface was the same as found in the as-quenched condition. Figure 27 reveals the shallow-dimpled rupture appearance of the fast feature area, characteristic of the high fracture toughness (39). This, too, was similar to the appearance of the fracture surface of as-quenched specimens.

5. Microstructure and Fatigue Crack Growth Rates After Tempering at 300°C

Tempering at 300°C led to a significant drop in yield strength, as well as to a drop in fracture toughness, as shown in Figs. 15 and 16. Transmission electron microscopy revealed that substantial growth of lath boundary precipitates had occurred (2). The lath boundary precipitation led to a change in appearance in the fast fracture area. There was a change from dimpled rupture, characteristic of the 225°C tempered specimen, to quasi-cleavage. Figure 28 shows a scanning electron micrograph of a surface in the fast fracture region. Quasi-cleavage fracture features are evident in the figure. The fatigue crack growth rates did not reflect the same deterioration as the fracture toughness. They did, in fact, improve slightly. The fatigue fracture surface appearance was unchanged as shown in Fig. 29, and the coefficient, m, remained approximately 2 (1.9). There was no increase in growth rates even when maximum stress intensity, K_{max}, approached K_{IC}.

The deterioration of fracture toughness in the 260-315°C tempering range was due to tempered martensite embrittlement. The structural features causing tempered martensite embrittlement were unexpectedly found to lead to a reduction in crack propagation rates in this steel. A similar discrepancy between toughness and crack growth rates was observed by Anctil and Kula in 4340 steel (37). Because the fatigue crack growth properties are not deleteriously affected by the presence of lath boundary precipitates it can be concluded that some of the microstructural features controlling fracture toughness do not affect the fatigue crack propagation in the same manner. Plastic deformation of the matrix is a requisite feature of fatigue crack growth, and for a given set of test conditions,

the characteristics of the matrix largely govern the crack growth rates. The influence of brittle particles is unclear; there is conflicting evidence on the role of such particles (40-42). Pelloux (41) found increased growth rates in aluminum alloys with increased particle density, but in his experiments the changes in particle density were large. Glassman and McEvily (42) found decreased rates in aluminum alloys with an increase in particle density. This work, however, was carried out at very high stresses with thin sheets and under conditions of plane stress.

Static fracture does not necessarily require plastic deformation; failure may be by cleavage. Fracture is highly sensitive to microstructural features, especially those offering easy crack paths, as was illustrated earlier for AISI 4340 steel. Thus, it is not surprising that certain heat treating procedures may cause a severe drop in fracture toughness without appreciably changing fatigue crack growth behavior.

6. Microstructure and Fatigue Crack Growth After Tempering at 500°C

Tempering at 500°C led to a small increase in yield strength, as shown in Fig. 15. This increase was caused by secondary hardening. There was a concomitant drop in fracture toughness, as shown in Fig. 16. Transmission electron microscopy revealed Fe_3C precipitate networks at lath boundaries (2). Although no molybdenum carbides were detected, they were undoubtedly present in small quantities because the 600°C tempering treatment (discussed in detail later) produced substantial amounts of easily identified molybdenum carbide.

The fatigue crack growth rate increased considerably on tempering at 500°C. The exponent, m, was 2.55. Figure 30 shows the appearance of the fatigue region at ΔK of 31 ksi-in.$^{1/2}$. The corresponding crack

growth rate was 2.5×10^{-5} in./cycle. The composite photograph reveals that the fatigue surface contained features similar to those observed in the 300°C temper condition. It was concluded that the thickened and extensive cementite films, as well as alloy carbides, led to the observed increase in growth rates for the 500°C tempered specimen.

7. Microstructure and Fatigue Crack Growth After Tempering at 600°C

A large increase in yield strength and a further decrease in fracture toughness were observed for specimens tempered at 600°C. The results are shown in Fig. 15 and Fig. 16. Transmission electron microscopy revealed Mo_2C dispersed within the martensite laths; electron diffraction showed that Fe_3C was no longer present in specimens tempered at this temperature (2,43). Extensive precipitation was revealed by optical metallography, as shown in Fig. 31.

The fatigue crack growth rates increased significantly over those characteristic of specimens tempered at lower temperatures. As K_{max} approached K_{IC} the growth rates increased to very high values, as shown in Fig. 21. The exponent, m, increased to 4.5, and there was considerable scatter in the growth rate data. Scanning electron microscopy of the fatigue surface revealed the notable reasons for the increased crack growth rate and the cause of the larger scatter in the data. Figure 32 is a composite photograph of the fatigue surface taken from a specimen which exhibited a crack growth rate of 1×10^{-5} in./cycle at ΔK of 21.5 ksi in.$^{1/2}$. The figure shows that an integranular failure mode was present in the fatigue region, as well as the usual ductile mode characteristic of a fatigue fracture. In the low stress intensity ranges, the crack growth rate curves for specimens tempered at both

500°C and 600°C overlapped, suggesting a basic similarity in behavior in the lower stress range. The increase in growth rates and the large scatter for the 600°C tempered specimen can be attributed to the added intergranular mode of failure present during fatigue in the specimen tempered at 600°C. Similar observations have been made on other steels (44). Richie and Knott (45) saw the presence of grain boundary cracking during fatigue in "temper brittle" EN30A (embrittled at 580°C) under plane strain conditions. Richie and Knott also found an increase in the exponent describing the fatigue crack growth properties. The embrittling phenomenon, leading to the intergranular cracking, has been attributed to several mechanisms. One is the segregation of impurity elements to prior austenite grain boundaries (46). Precipitation at prior austenite grain boundaries could also lead to deteriorated properties by providing a nearly continuous film (47).

IV. SUMMARY AND CONCLUSIONS

The room temperature plane strain fracture toughness of AISI 4340 was greatly improved without the loss in strength levels in as-quenched and low-temperature tempered conditions when the austenitizing temperature was raised from 870°C to 1200°C. This improvement in fracture toughness with increase in austenitizing temperature was attributed to (a) the virtual elimination of twinned martensite plates and (b) the large increase in the amount of retained austenite films surrounding martensite laths.

When AISI 4340 steel, following austenitizing at 870°C (resulting in the austenite grain size ASTM 7-8) was tempered, there was no evidence of tempered martensite embrittlement in the room temperature plane strain fracture toughness measurements. This was in agreement with the investigations of other workers. However, embrittlement was observed after tempering at 280°C and 350°C in specimens of AISI 4340 steel that were austenitized at 1200°C (resulting in the austenite grain size ASTM 0-1). The distribution and morphology of cementite platelets both at lath boundaries and prior austenite grain boundaries, resulting from tempering at 280°C, were similar for the two austenitizing treatments. The discrete precipitation of cementite at prior austenite grain boundaries was observed in both cases. The fracture mode of the embrittled 1200°C austenitized specimen was intergranular along prior austenite grain boundaries, while that of the unembrittled 870°C austenitized specimen was transgranular and consisted of both dimpled rupture and quasi-cleavage. Thus, the microstructural and fracture surface observations failed to resolve the difference in fracture behavior between the embrittled 1200°C

austenitized specimen and the unembrittled 870°C austenitized specimens.

From a study of the results reported in the literature and the evidence obtained in the present investigation, it was concluded that detection of tempered martensite embrittlement was dependent on many factors such as loading rate (static or dynamic loading), testing temperature, austenite grain size, and specimen geometry. The observed embrittlement in the 1200°C austenitized specimens (after tempering at 280°C and 350°C) was believed to be associated with the large austenite grains which possibly enhanced detection (or severity) of tempered martensite embrittlement in room temperature tests by raising the fracture toughness transition temperature.

The fatigue crack growth properties and fracture toughness properties for the 5 Mo-0.3 C steel are compared for the different tempering treatments in Fig. 33 (the crack growth properties are shown as the number of cycles to grow one inch at a given ΔK). This figure clearly shows that there was no unique relation between fatigue crack growth rates and fracture toughness. Specimens tempered at 300°C had lower values of fracture toughness, whereas they exhibited a reduction in crack growth rate when compared with specimens tempered at 225°C.

The general conclusions gleened from the study of fatigue crack propagation in 5 Mo-0.3 C steel are summarized below:

(1) Microstructural changes during tempering of quenched steels can lead to drastic changes in fatigue crack growth rates.

(2) The microstructural features affecting fracture toughness do not always affect fatigue crack propagation in the same way. There is no unique relationship between fracture toughness and crack

growth rates that holds for all microstructures. In the case of 5 Mo-0.3 C steel, cementite precipitation at lath boundaries lowered fracture toughness while having no deleterious effect on the fatigue crack growth rates. When the carbide precipitation became more extensive, however, both properties deteriorated.

(3) The presence of additional failure modes in the fatigue area, such as intergranular fracture, causes an increase in crack growth rates, as characterized by the empirical constants in the Paris equation.

(4) The fatigue crack growth properties of as-quenched 5 Mo-0.3C steel, which had an autotempered martensitic structure, were generally good, particularly at high values of ΔK. The crack growth rates followed an approximate second power dependence.

ACKNOWLEDGEMENTS

The authors gratefully acknowledge the valuable help of Dr. M. Dilip Bhandarkar for his critical review of the manuscript.

This research was performed partially under the auspices of the U. S. Atomic Energy Commission through the Inorganic Materials Research Division of the Lawrence Berkeley Laboratory, and partially under the auspices of the Army Materials and Mechanics Research Center, Watertown, MA, Contract No. DAAG46-73-C-0120.

REFERENCES

1. W. E. Wood, E. R. Parker and V. F. Zackay, An Investigation of Metallurgical Factors which Affect the Fracture Toughness of Ultra High Strength Steels (D. Eng. Thesis), LBL-1474, Lawrence Berkeley Laboratory, University of California, May 1973.
2. R. D. Goolsby, Relationships Between Microscostructure and Fracture Toughness in a Secondary Hardening Steel (Ph. D. Thesis), LBL-405, Lawrence Berkeley Laboratory, University of California, November 1971.
3. Annual Book of ASTM Standards, E 399-72, American Society for Testing and Materials, Philadelphia, 1973, p. 960.
4. J. E. Srawley and B. Gross, Mater. Res. Stand. 7, 155 (1967).
5. A. J. Baker, F. J. Lauta and R. P. Wei, ASTM STP 370, American Society for Testing and Materials, Philadelphia, 1963, p. 3.
6. E. B. Kula and A. A. Anctil, J. of Materials 4(4), 817 (1969).
7. G. Krauss and A. R. Marder, Met. Trans. 2, 2343 (1971).
8. J. M. Marder and A. R. Marder, Trans. ASM 62, 1 (1969).
9. W. S. Owen, E. A. Wilson and T. Bell, High Strength Materials, V. F. Zackay, ed (John Wiley and Sons, New York, 1965), p. 167.
10. E. Tekin and P. M. Kelly, Precipitation from Iron-Base Alloys (AIME, New York, 1965).
11. P. M. Kelly and J. Nutting, J. Iron Steel Inst. 197, 199 (1961).
12. M. G. H. Wells, Acta Met. 12, 389 (1964).
13. S. K. Das and G. Thomas, Trans. ASM 62, 659 (1969).
14. Der-Hung Huang and G. Thomas, Met. Trans. 2, 1587 (1971).
15. C. Krauss and W. Pitsch, Acta Met. 12, 278 (1964).

16. M. Bevis, P. C. Rowlands and A. F. Acton, Trans. TMS-AIME 242, 1555 (1968).

17. A. Gilbert, G. T. Hahn, C. N. Reid and B. A. Wilcox, Acta Met. 12, 754 (1964).

18. D. Webster, Trans. ASM 61, 816 (1968).

19. M. A. Grossmann, Trans. TMS-AIME 167, 39 (1946).

20. R. L. Rickett and J. M. Hodge, Proc. ASTM 51, 931 (1951).

21. L. J. Klingler, W. J. Barnett, R. P. Frohmberg and A. R. Troiano, Trans. ASM 46, 1557 (1954).

22. W. A. Backofen and M. L. Ebner, Metallurgical Aspects of Fracture at High Strength Levels, WAL TR 310.24/5-4, 1963, Army Materials and Mechanics Research Center, Watertown, Mass.

23. M. F. Amateau and E. A. Steigerwald, Fracture Characteristics of Structural Metals, Contract Now-64-0186C, 1965, U. S. Bureau of Naval Weapons.

24. F. J. Lauta and E. A. Steigerwald, Influence of Work Hardening Coefficient on Crack Propagation in High Strength Steels, AFML-TR-65-31, 1965, Air Force Materials Laboratory, Dayton, Ohio.

25. W. G. Ferguson and M. N. Sargisson, Eng. Fract. Mech. 5, 499 (1973).

26. T. M. F. Ronald, Met. Trans. 1, 2583 (1970).

27. E. A. Steigerwald, Eng. Fract. Mech. 1, 473 (1969).

28. B. S. Lament, B. L. Averbach and M. Cohen, Trans. ASM 46, 851 (1954).

29. B. R. Banerjee, J. Iron Steel Inst. 203, 166 (1965).

30. C. J. Alstetter, M. Cohen and B. L. Averbach, Trans. ASM 55, 287 (1962).

31. G. Y. Lai, W. E. Wood, E. R. Parker and V. F. Zackay, in preparation.

32. J. M. Capus and G. Mayer, Metallurgia, 62, 133 (1960).

33. P. Paris and F. Erdogan, Trans. ASME 85, 528 (1963).

34. J. Mandel, The Statistical Analysis of Experimental Data (Wiley-Interscience, New York, 1964), p. 247.

35. P. R. Evans, N. B. Owens and B. E. Hopkins, Eng. Fract. Mech. 3, 463 (1971).

36. F. A. Heiser and W. Mortimer, Met. Trans. 3, 2119 (1972).

37. A. A. Anctil and E. B. Kula, Effects of Environment and Complex Load History on Fatigue Life, ASTM STP 462, American Society for Testing and Materials, Philadelphia, 1970, p. 297.

38. J. F. Throop and G. A. Miller, Achievement of High Fatigue Resistance in Metals and alloys, ASTM STP 467, American Society for Testing and Materials, Philadelphia, 1970, p. 154.

39. C. D. Beachem and R. M. N. Pelloux, Fracture Toughness Testing and Its Applications, ASTM STP 381, American Society for Testing and Materials, Philadelphia, 1965, p. 210.

40. C. Laird, Fatigue Crack Propagation, ASTM STP 415, American Society for Testing and Materials, Philadelphia, 1967, p. 131.

41. R. M. N. Pelloux, Trans. ASM 57, 511 (1964).

42. L. H. Glassman and A. J. McEvily, Jr., National Aeronautics and Space Administration TN D-928, 1962.

43. D. Raynor, J. A. Whiteman and R. W. K. Honeycombe, J. Iron Steel Inst. 204, 349 (1966).

44. C. E. Richards and T. C. Lindley, Eng. Fract. Mech. 4, 951 (1972).

45. R. O. Richie and J. F. Knott, Acta Met. 21, 639 (1973).

46. J. R. Low, Jr., Trans. TMS-AIME 245, 2481 (1969).

47. J. Plateau, G. Henry and C. Crussard, Rev. Metall. 54, 200 (1957).

Table I. Chemical analyses of Mo-C Steels

Alloy No.	Mo	Mn	C	Fe
723-15	5.0	0.66	0.28	balance
723-16	5.1	0.70	0.26	balance
723-18	5.2	0.62	0.28	balance

FIGURE CAPTIONS

Fig. 1. Effect of austenitizing and tempering temperatures on strength and fracture toughness of AISI 4340 steel.

Fig. 2. Scanning electron micrographs of the fracture surfaces of as-quenched AISI 4340 steel specimens austenitized at (a) 870°C showing dimples and quasi-cleavage facets and (b) 1200°C showing predominantly dimples.

Fig. 3. Scanning electron micrographs of fracture surface of AISI 4340 steel specimens tempered at 280°C after austenitizing at (a) 870°C, showing a mixture of dimples and quasi-cleavage facets, and (b) 1200°C, showing predominantly intergranular fracture.

Fig. 4. As-quenched structure of specimens of AISI 4340 steel. (a) Optical micrograph, and (b) transmission electron micrograph, showing a mixture of martensite laths and plates for the 870°C austenitizing treatment. (c) Optical micrograph showing both martensite plates nucleating from prior austenite grain boundaries and martensite laths within prior austenite grains, and (d) transmission electron micrograph showing martensite laths for the 1200°C→870°C austenitizing treatment. Some martensite plates are marked P and the internal twins in martensite laths are indicated by small arrows.

Fig. 5. Transmission electron micrographs of martensite plates in as-quenched AISI 4340 steel austenitized at 870°C, showing extensive fine transformation twins.

Fig. 6. Transmission electron micrographs of a twinned martensite plate in the as-quenched specimen of AISI 4340 steel austenitized at 870°C. (a) Bright field image showing the $\{112\}_M$ transformation twins and the electron diffraction pattern showing both the matrix and twin diffraction patterns, (b) dark field image of twin spot indicated by the arrow) showing the reversal of contrast of the twins.

Fig. 7. Transmission electron micrograph of a martensite plate (marked P) in as-quenched AISI 4340 steel austenitized at 1200°C showing the absence of the transformation twins. The plates contained numerous cross-hatched ε carbides formed during quenching.

Fig. 8. Transmission electron micrographs of as-quenched AISI 4340 steel: (a) bright field, and (b) dark field of austenite reflection, for the 870°C austenitizing treatment.

Fig. 9. Transmission electron micrographs of as-quenched AISI 4340 steel specimen, austenitized at 1200°C, showing extensive amounts of retained austenite films surrounding martensite laths: (a) bright field image, (b) dark field image of the (002) austenite reflection showing reversal contrast of retained austenite films. (c) Selected area diffraction pattern (d) schematic sketch of the selected area diffraction pattern with austenite (γ) and martensite (M) reflections indexed.

Fig. 10. Typical autotempered martensite in an as-quenched specimen of AISI 4340 steel austenitized at 1200°C: (a) bright field image, (b) dark field image of cementite reflection showing fine cementite precipitate within martensite laths. These micrographs are also representative of autotempered martensite in the steel austenitized at 870°C.

Fig. 11. Typical transmission electron micrographs showing autotempered martensite containing ε carbide which forms on $\{100\}_\alpha$ planes and along $\langle 100 \rangle_\alpha$ directions in as-quenched AISI 4340 steel austenitized at (a) 870°C and (b) 1200°C.

Fig. 12. Dark field micrographs formed from a cementite reflection showing the precipitation of cementite both at lath boundaries and within the laths in AISI 4340 steel specimens tempered at 280°C after austenitizing at (a) 870°C and (b) 1200°C.

Fig. 13. Transmission electron micrograph of a specimen of AISI 4340 steel tempered at 280°C after austenitizing at 870°C, showing discrete precipitation of cementite platelets at prior austenite grain boundaries (marked GB).

Fig. 14. Transmission electron micrographs of a specimen of AISI 4340 steel tempered at 280°C after austenitizing at 1200°C showing discrete precipitation of cementite platelets at prior austenite grain boundaries (marked GB): (a) bright field image, (b) dark field image of a cementite reflection.

Fig. 15. Room temperature strength as a function of tempering temperature for 5 Mo-0.3 C steel.

Fig. 16. Room temperature plane strain fracture toughness as a function of tempering temperature for 5 Mo-0.3 C steel.

Fig. 17. Fatigue crack propagation rate vs stress intensity range for the as-quenched 5 Mo-0.3 C steel. Data from specimens 15-1 and 18-1.

Fig. 18. Fatigue crack parpagation rate vs stress intensity range for the 225°C tempered 5 Mo-0.3 C steel. Data from specimens 16-2 and 18-2.

Fig. 19. Fatigue crack propagation rates vs stress intensity range for the 300°C tempered 5 Mo-0.3 C steel. Data from specimens 15-3 and 16-3.

Fig. 20. Fatigue crack propagation rates vs stress intensity range for the 500°C tempered 5 Mo-0.3 C steel. Data from specimens 15-4 and 18-4.

Fig. 21. Fatigue crack propagation rates vs stress intensity range for the 600°C tempered 5 Mo-0.3 C steel. Data from specimen 15-5.

Fig. 22. Microstructure of as-quenched 5 Mo-0.3 C steel.

Fig. 23. Transmission electron micrographs of as-quenched 5 Mo-0.3 C steel showing in bright field (a) autotempered, dislocated martensite laths, and in dark field (b) cementite precipitation.

Fig. 24. Scanning electron micrographs of fatigue fracture region in as-quenched 5 Mo-0.3 C steel. (a) Overall appearance of surface. ΔK-35 ksi-in.$^{1/2}$. (b) Composite enlargement showing quasi-cleavage at A, fatigue cracking through bulk microstructure at B, and local striations at C.

Fig. 25. Scanning electron micrographs of fatigue fracture showing striations in as-quenched 5 Mo-0.3 C steel. (a) Overall appearance of fatigue surface. ΔK = 40 ksi-in.$^{1/2}$. Striations appear at A. (b) Enlargement of striations.

Fig. 26. Comparison of fatigue crack propagation rate vs stress intensity range of as-quenched 5 Mo-0.3 C steel with rates reported for

other high-strength steels (A-Ref. 36, B-Ref. 37, C-Ref. 38 and D-Ref. 35).

Fig. 27. Scanning electron micrograph of fast fracture appearance of 225°C tempered 5 Mo-0.3 C steel showing primarily dimpled rupture characteristics.

Fig. 28. Scanning electron micrograph of fast fracture appearance of 300°C tempered 5 Mo-0.3 C steel showing quasi-cleavage characteristics.

Fig. 29. Composite of scanning electron micrographs showing fatigue fracture surface of 300°C tempered 5 Mo-0.3 C steel. General fatigue appearance resembles that of as-quenched material. $\Delta K = 35$ ksi-in.$^{1/2}$.

Fig. 30. Composite scanning electron micrograph showing fatigue fracture surface of 500°C tempered 5 Mo-0.3 C steel. Quasi-cleavage visible. $\Delta K = 31$ ksi-in.$^{1/2}$.

Fig. 31. Microstructure of 600°C tempered 5 Mo-0.3 C steel.

Fig. 32. Composite scanning electron micrograph showing fatigue fracture surface of 600°C tempered 5 Mo-0.3 C steel. Intergranular mode of failure evident in fatigue area. $\Delta K = 21$ ksi-in.$^{1/2}$.

Fig. 33. Comparison of fatigue crack growth and fracture toughness properties of 5 Mo-0.3 C steel for the different tempering treatments. Number of cycles to grow one inch at a constant stress intensity range are used to measure crack growth characteristics.

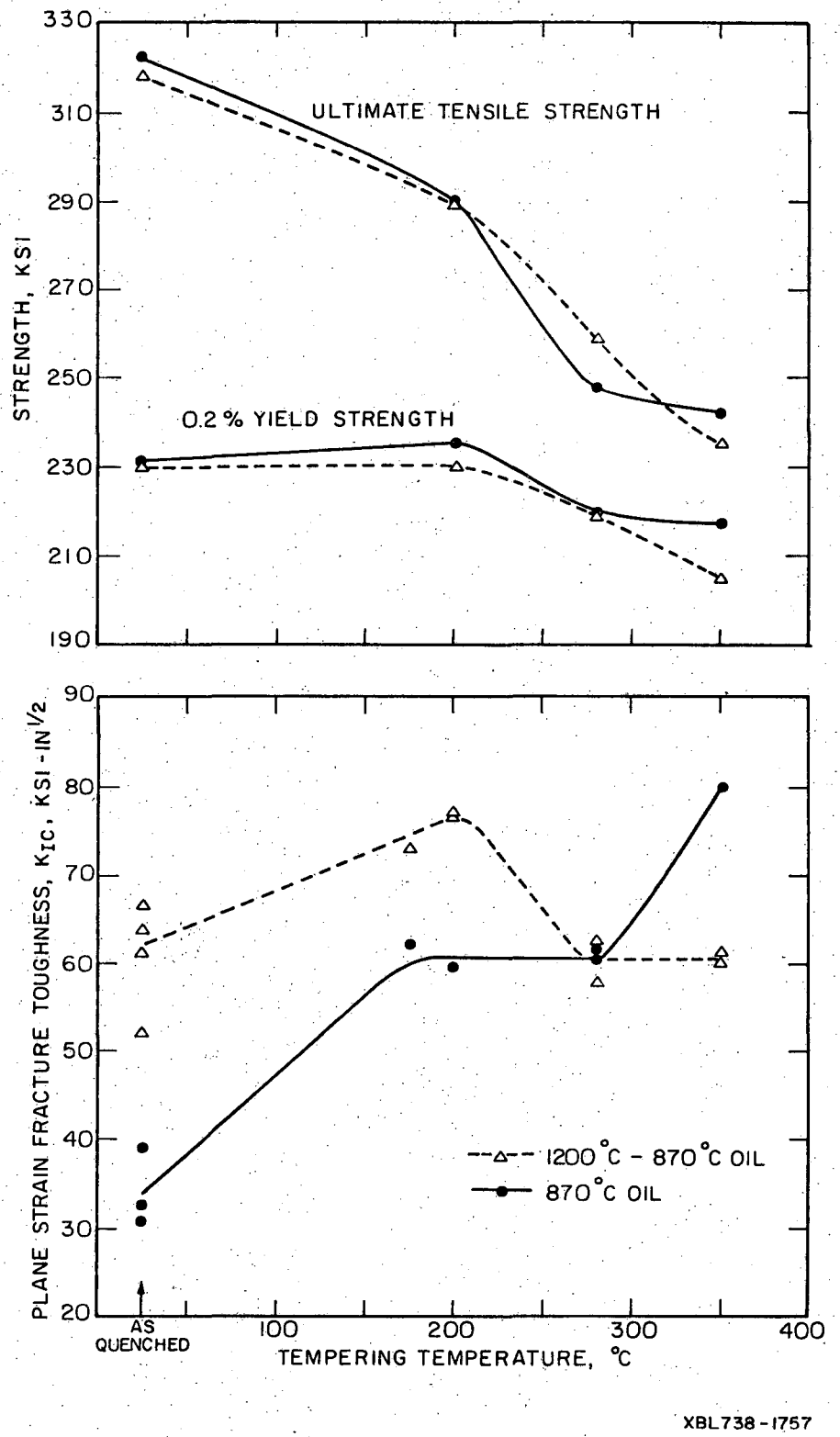
330
310
290
270
250
230
210
190
STRENGTH, KSI
ULTIMATE TENSILE STRENGTH
0.2 % YIELD STRENGTH
90
80
70
60
50
40
30
20
PLANE STRAIN FRACTURE TOUGHNESS, K_{IC}, KSI-IN$^{1/2}$
1200 °C - 870 °C OIL
870 °C OIL
AS QUENCHED
100
200
300
400
TEMPERING TEMPERATURE, °C
XBL738-1757

Fig. 1

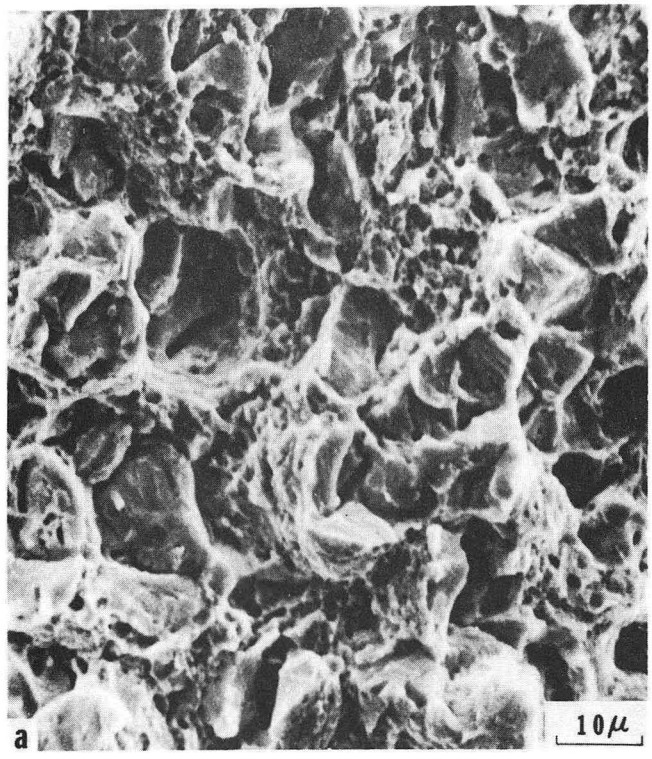

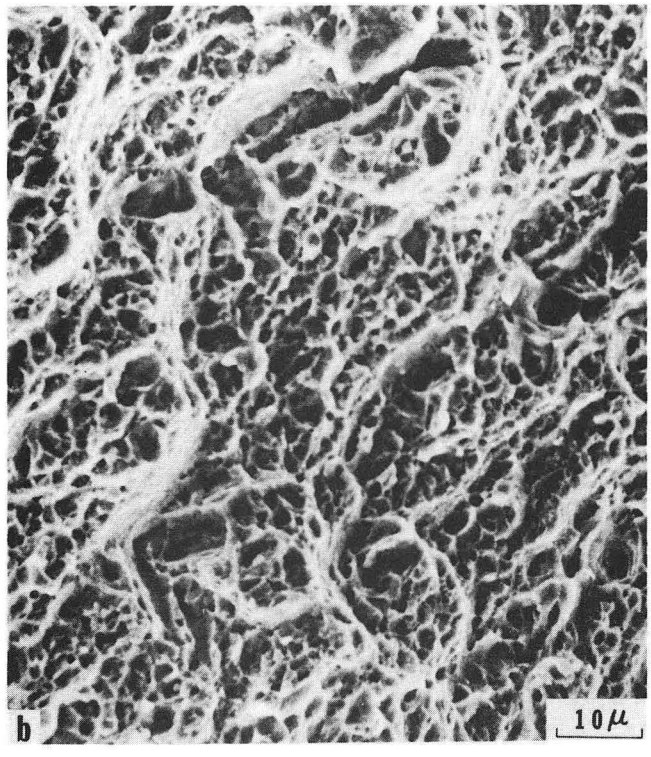

XBB 738-5024

Fig. 2

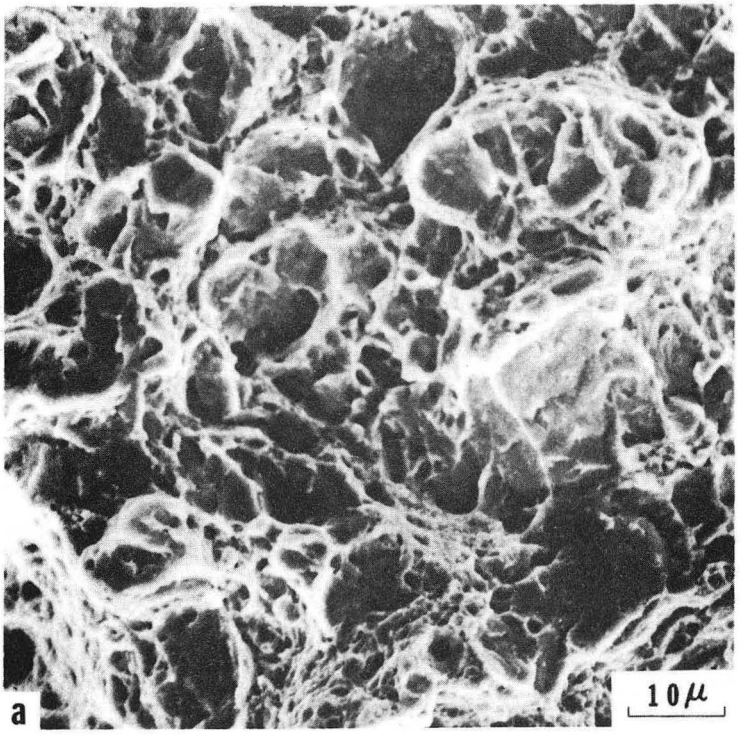

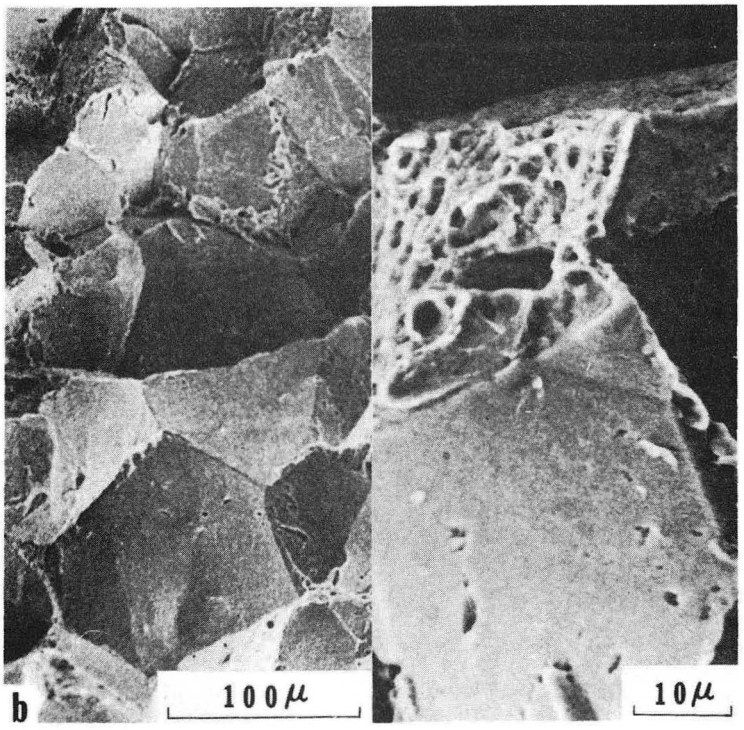

XBB 738-5019

Fig. 3

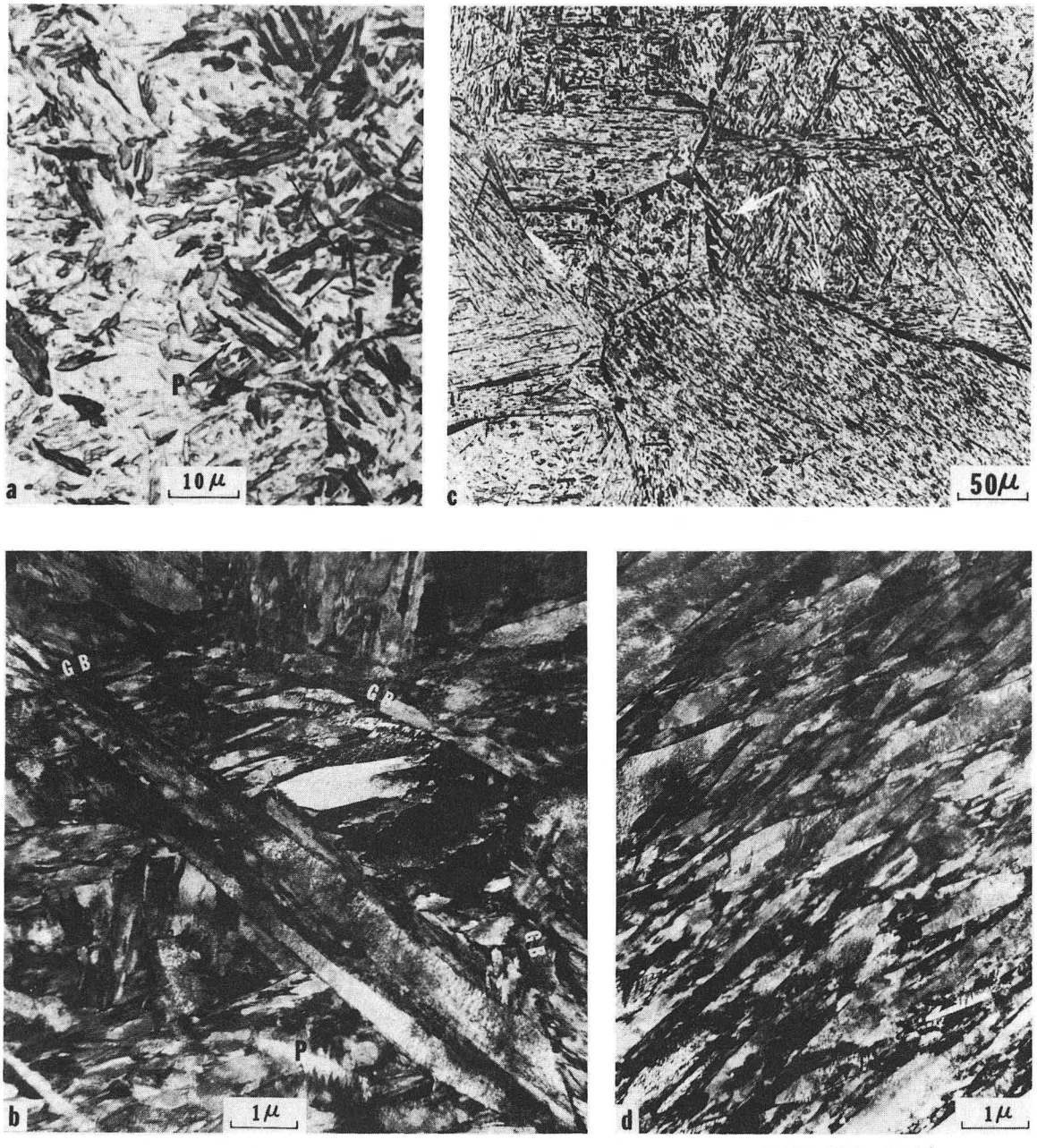

XBB 738-5014

Fig. 4

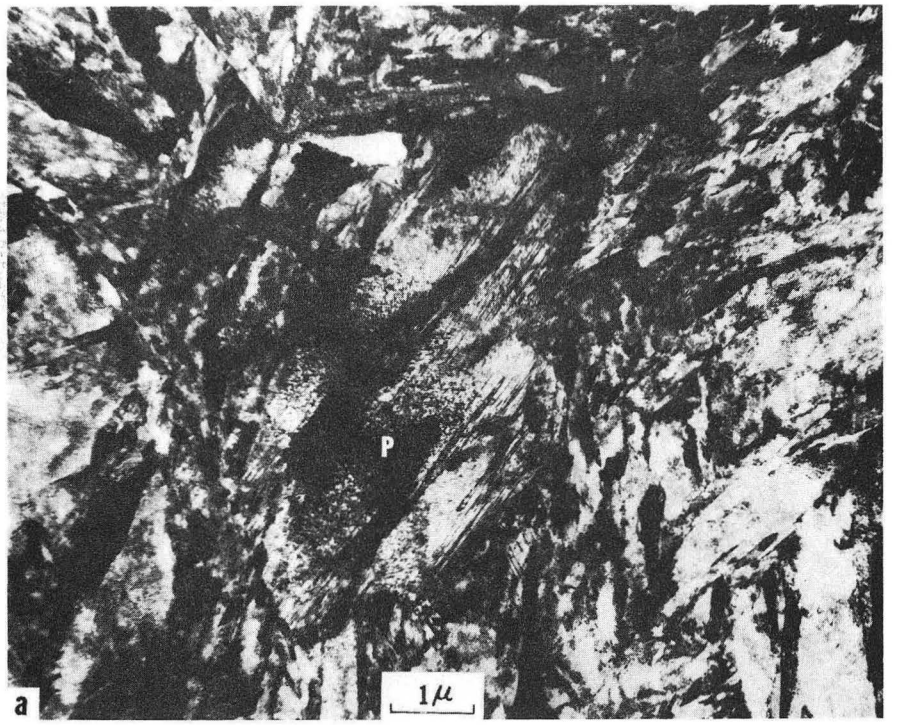

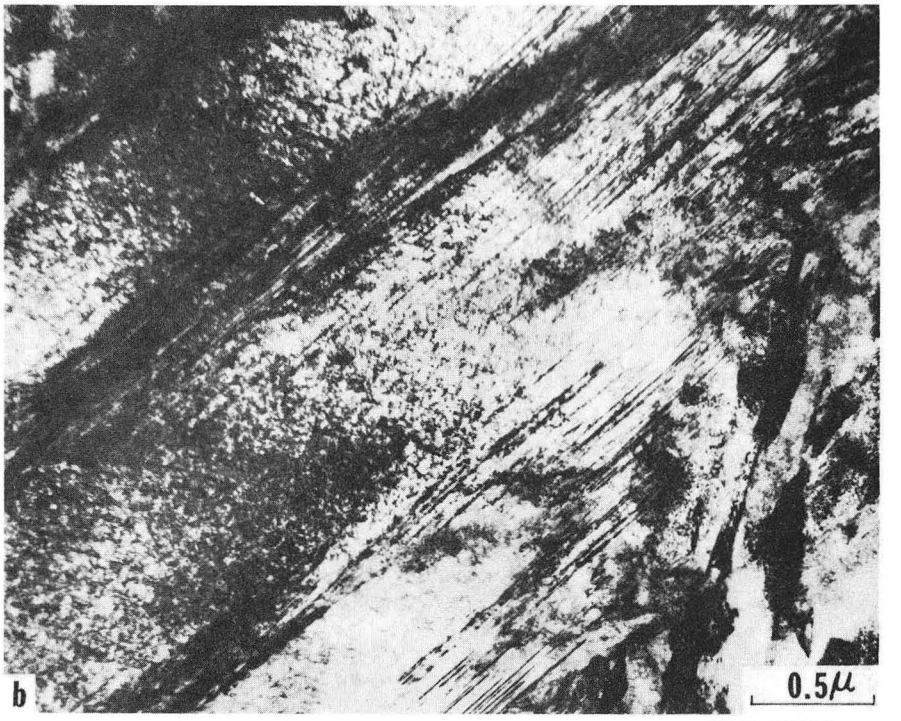

XBB 738-5018

Fig. 5

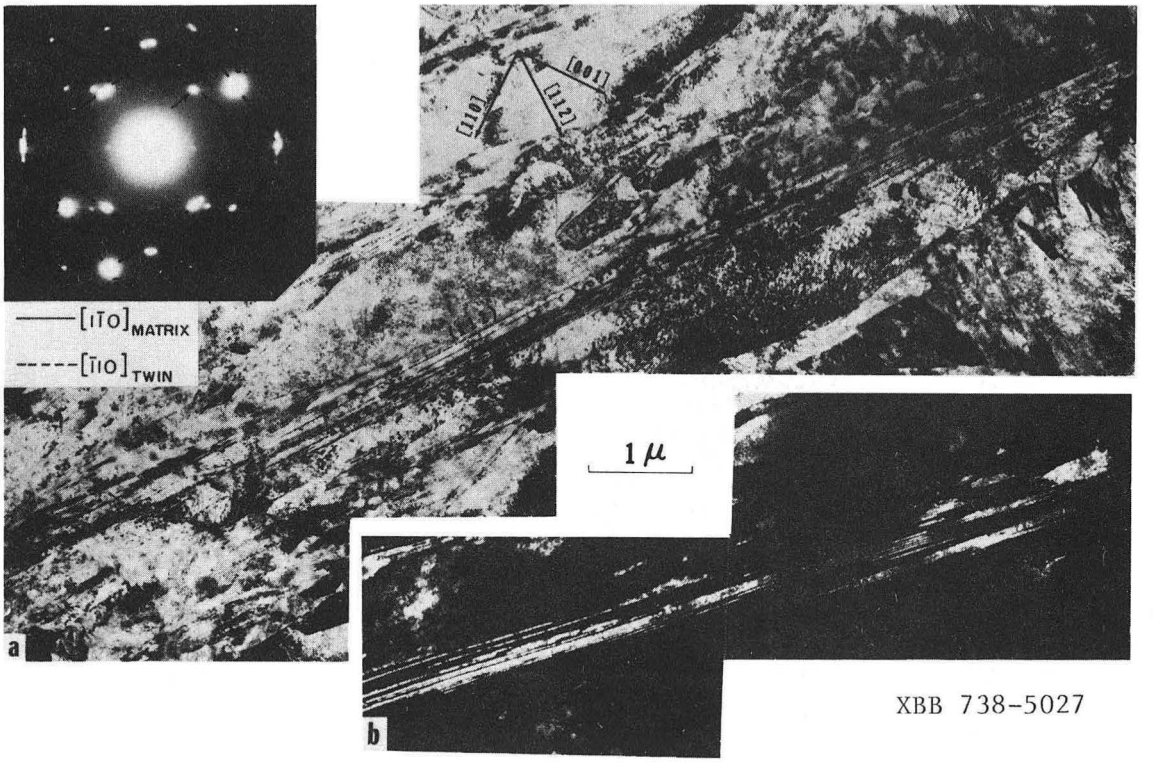

Fig. 6

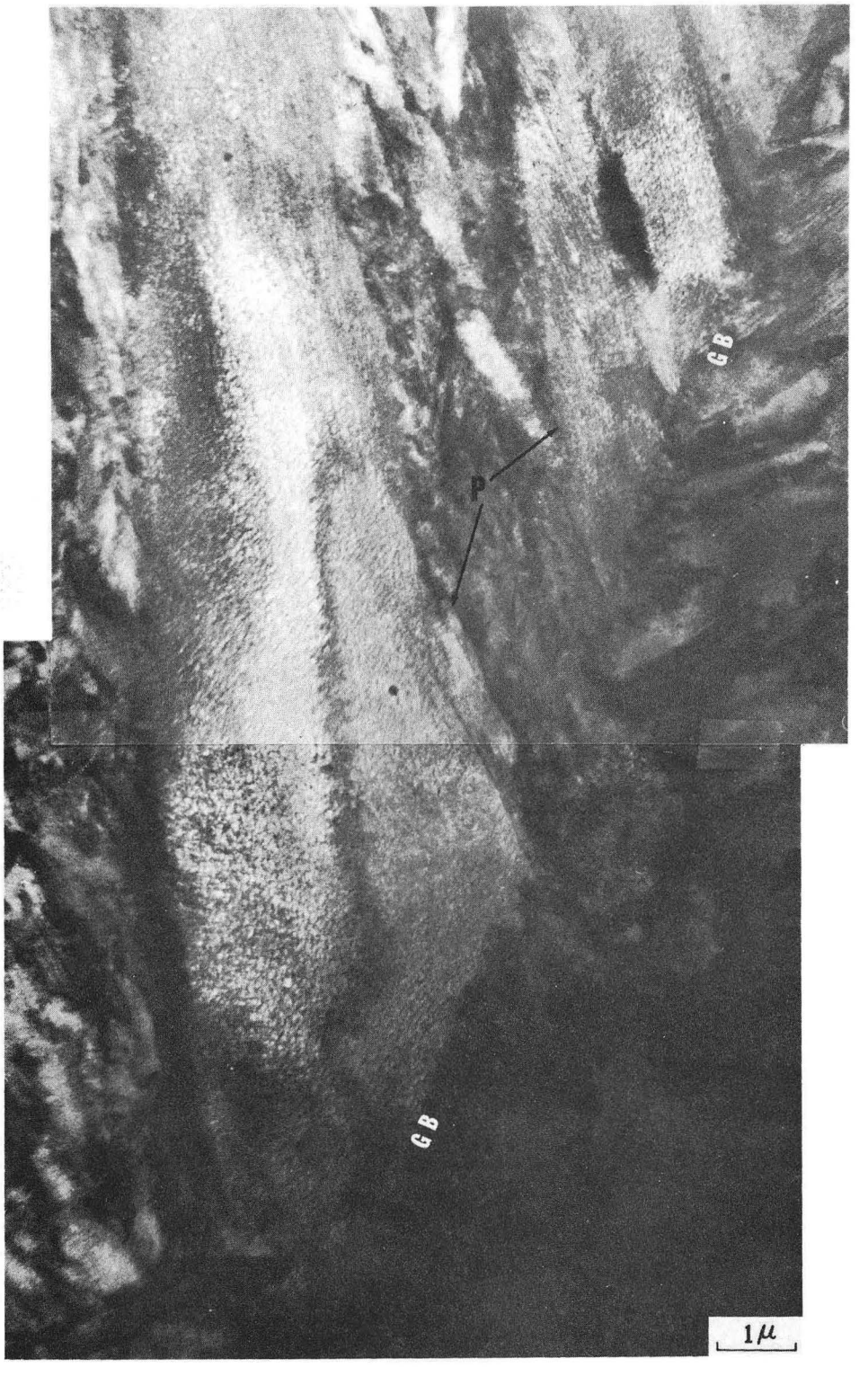

XBB 738-5028

Fig. 7

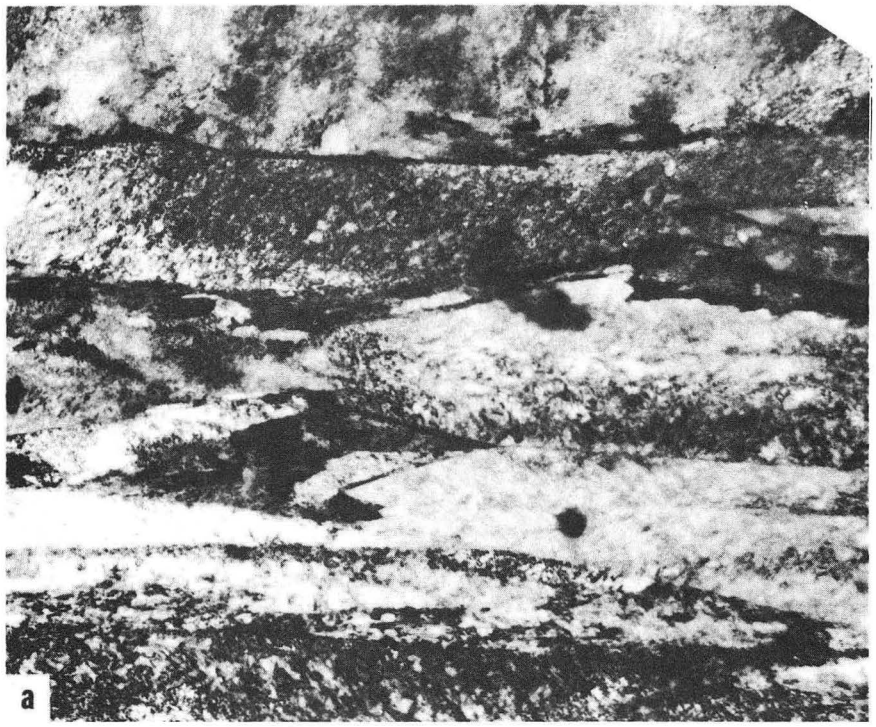

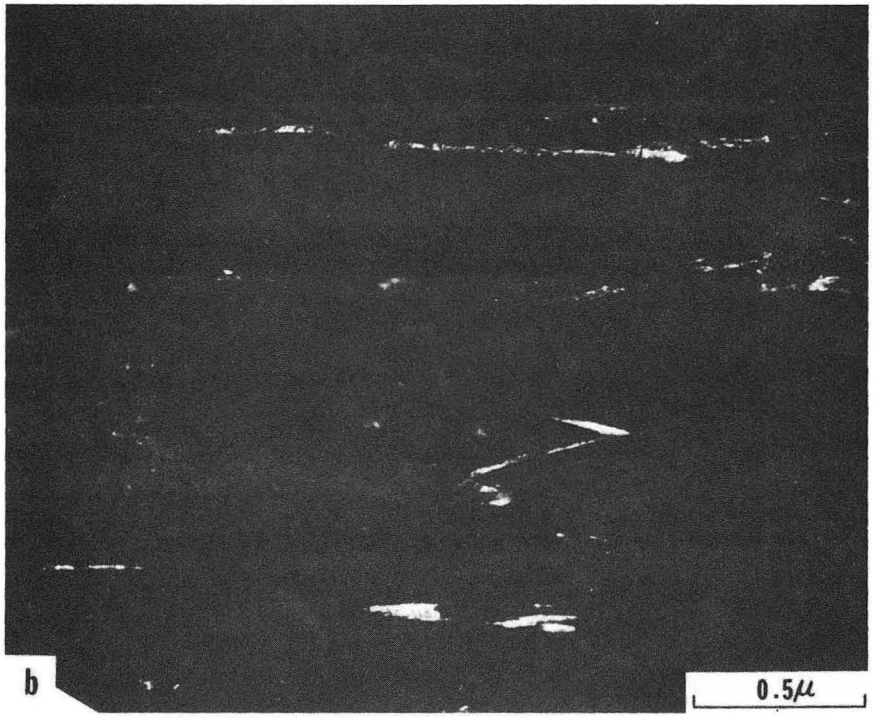

XBB 738-5026

Fig. 8

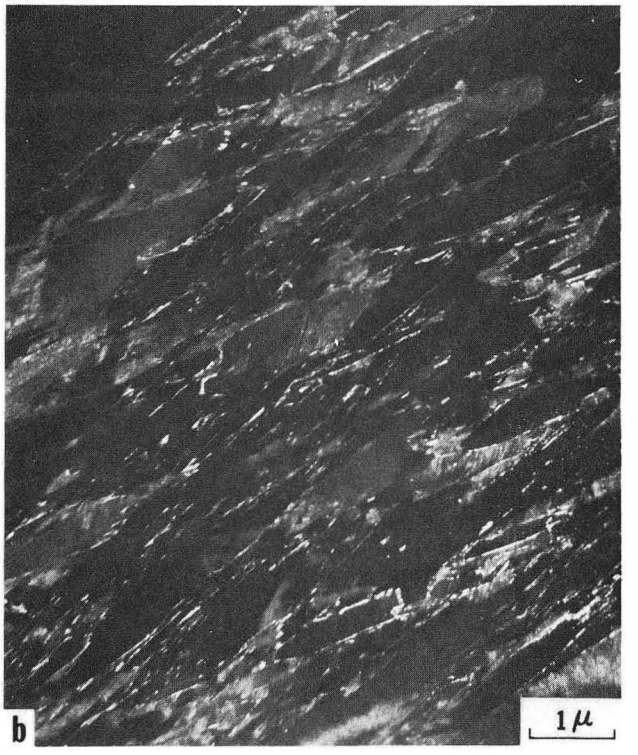

XBB 738-5025

Fig. 9

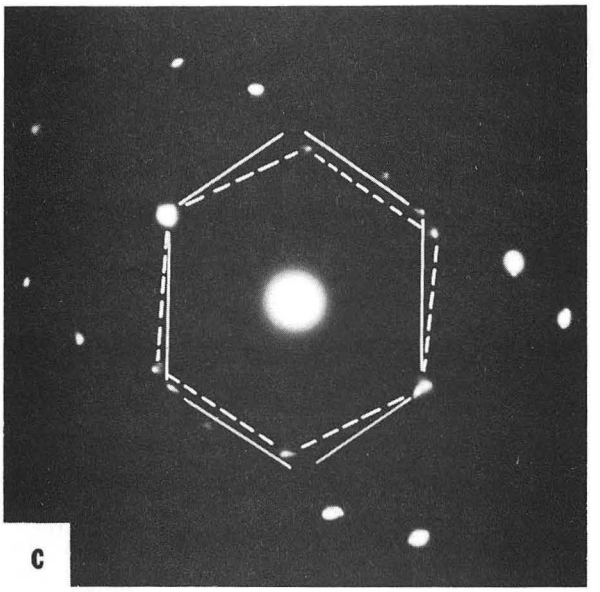

c

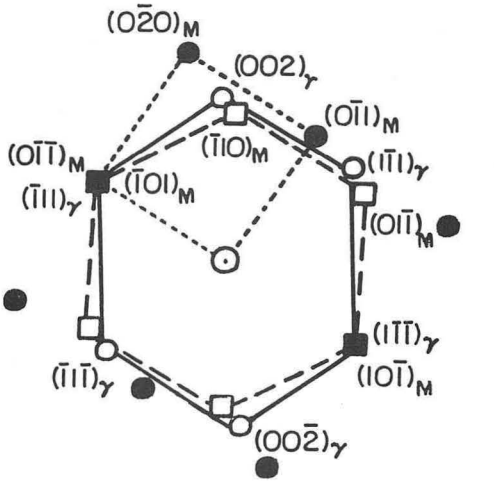

d

□ [111] MARTENSITE SPOT
○ [110] AUSTENITE SPOT
● [100] MARTENSITE SPOT

XBB 742-1250

Fig. 9 cont.

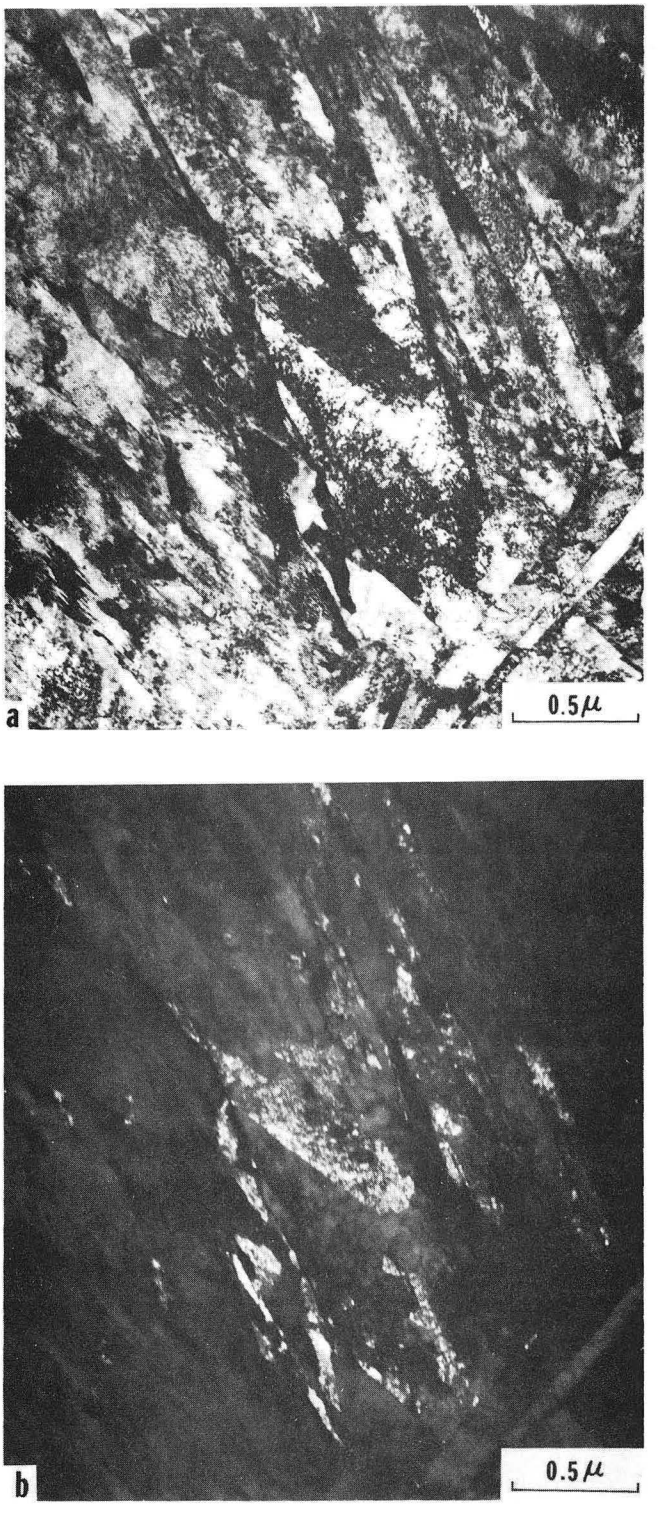

XBB 738-5021

Fig. 10

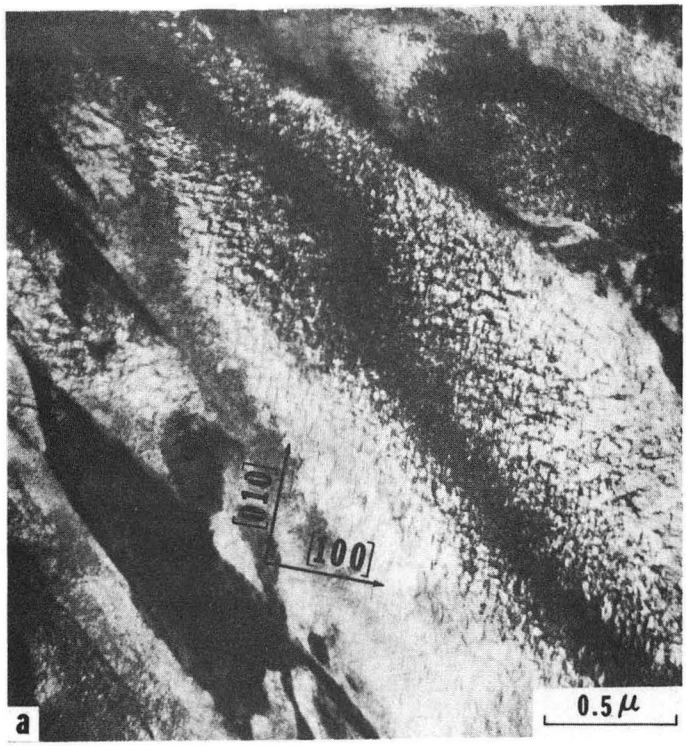

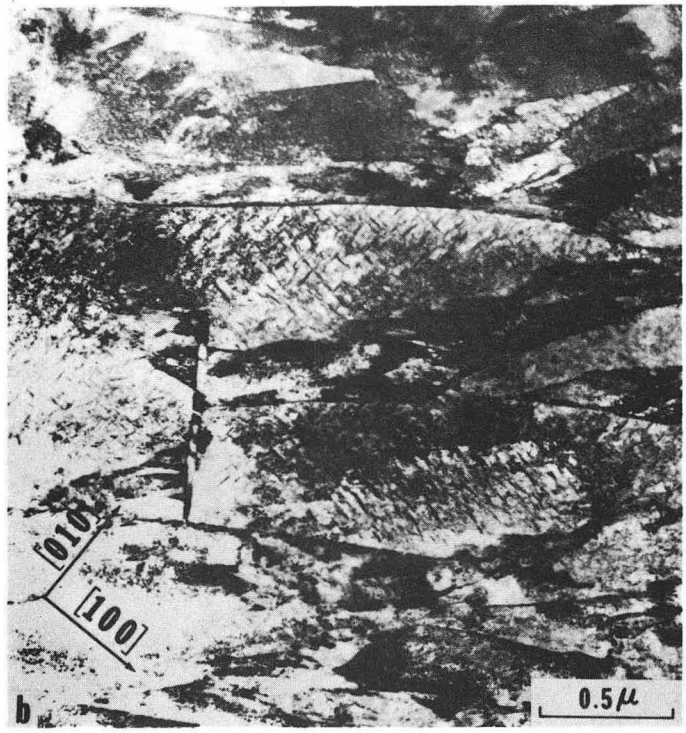

XBB 738-5022

Fig. 11

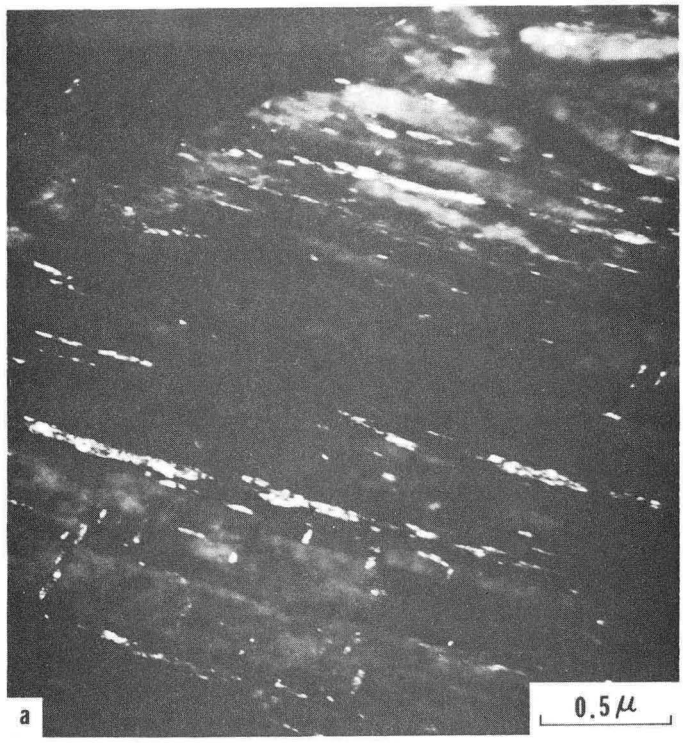

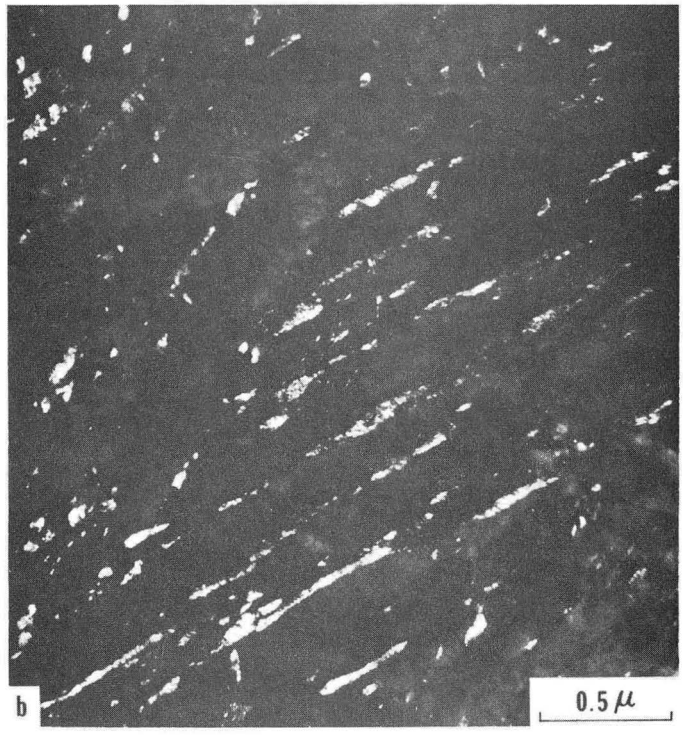

XBB 738-5023

Fig. 12

XBB 743-1694

Fig. 13

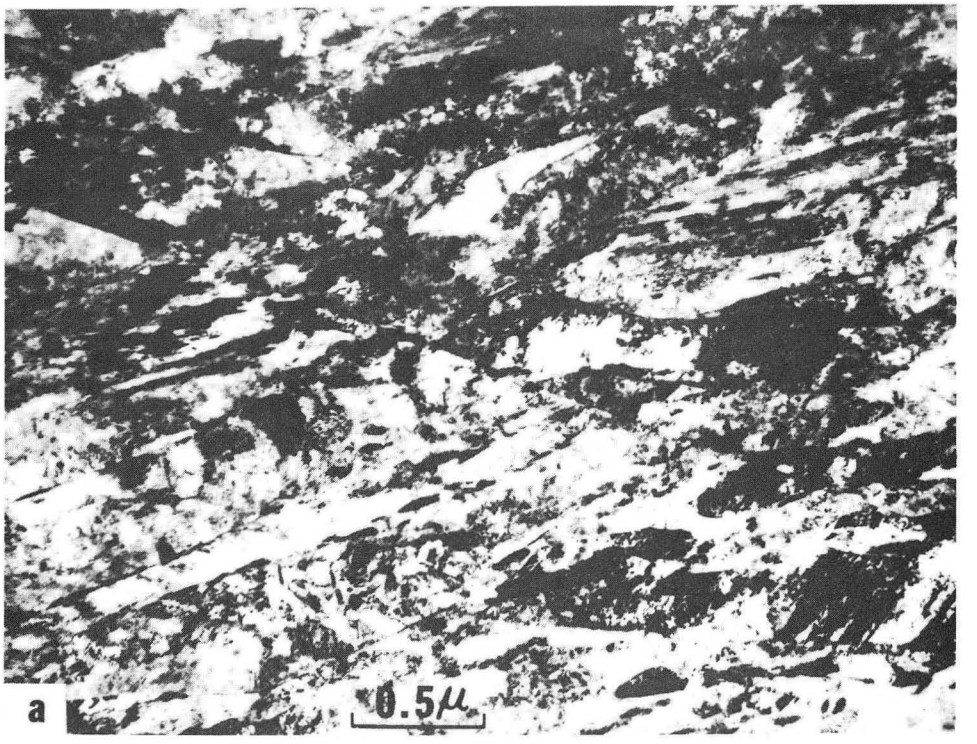

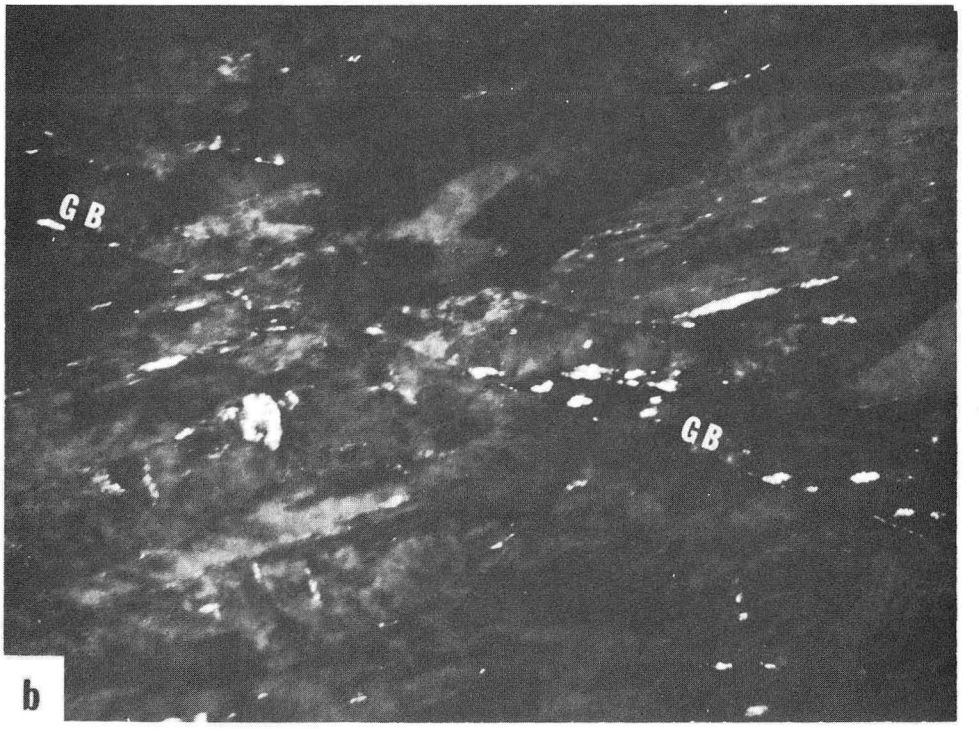

XBB 743-1695

Fig. 14

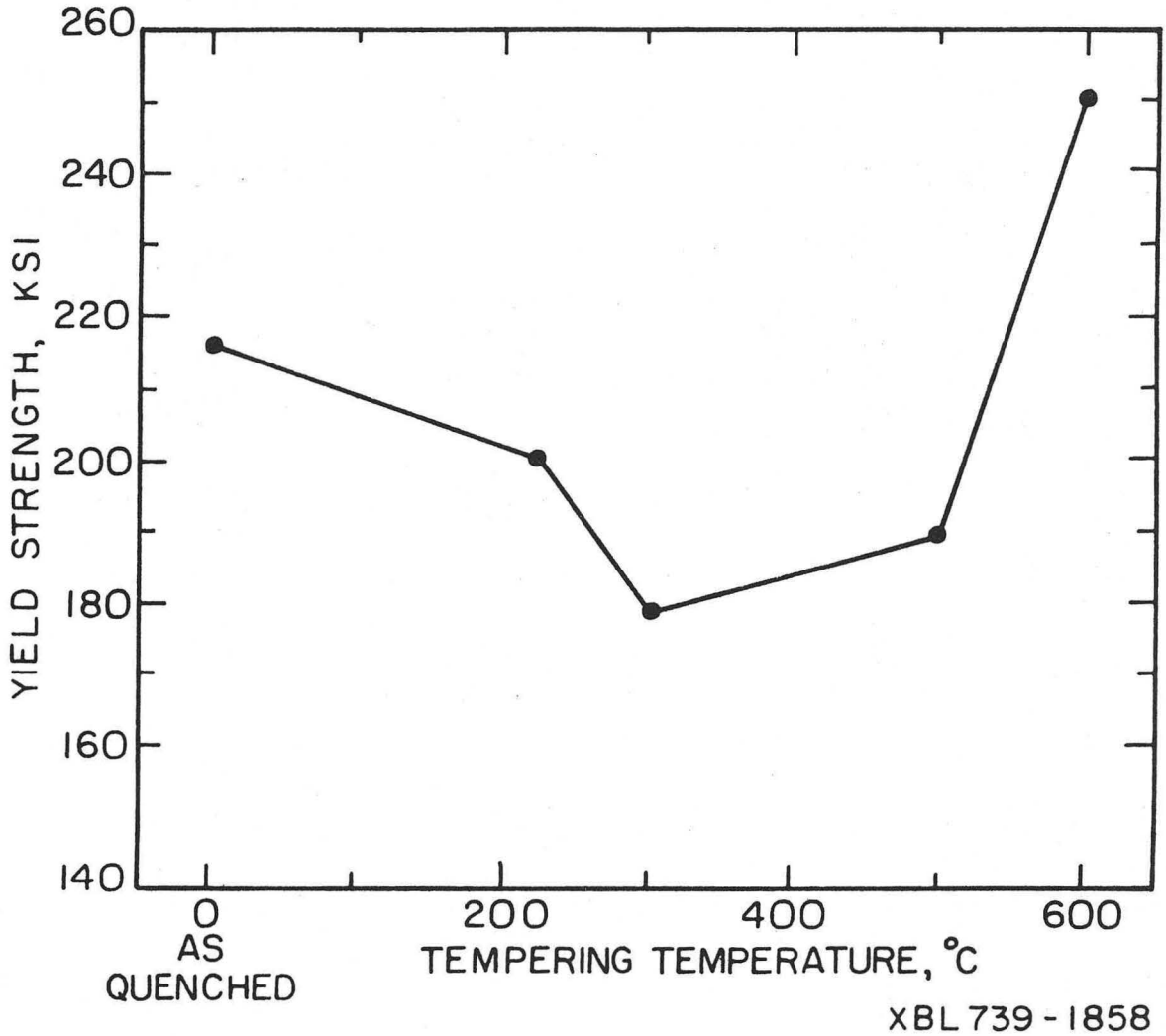
260
240
220
200
180
160
140
YIELD STRENGTH, KSI
0
AS
QUENCHED
200
400
600
TEMPERING TEMPERATURE, °C
XBL 739-1858

Fig. 15

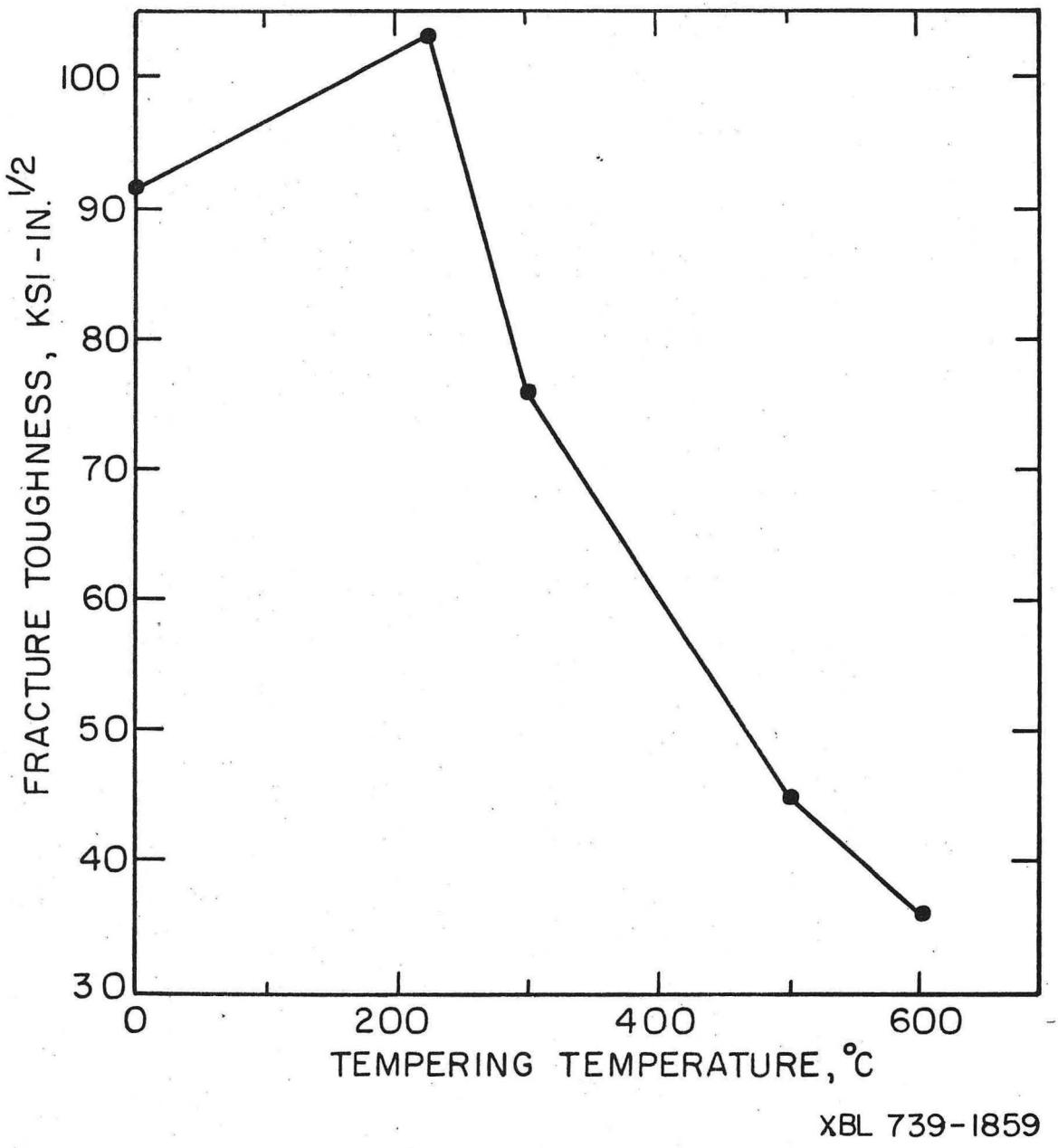
FRACTURE TOUGHNESS, KSI-IN.$^{1/2}$
100
90
80
70
60
50
40
30
0
200
400
600
TEMPERING TEMPERATURE, °C
XBL 739-1859

Fig. 16

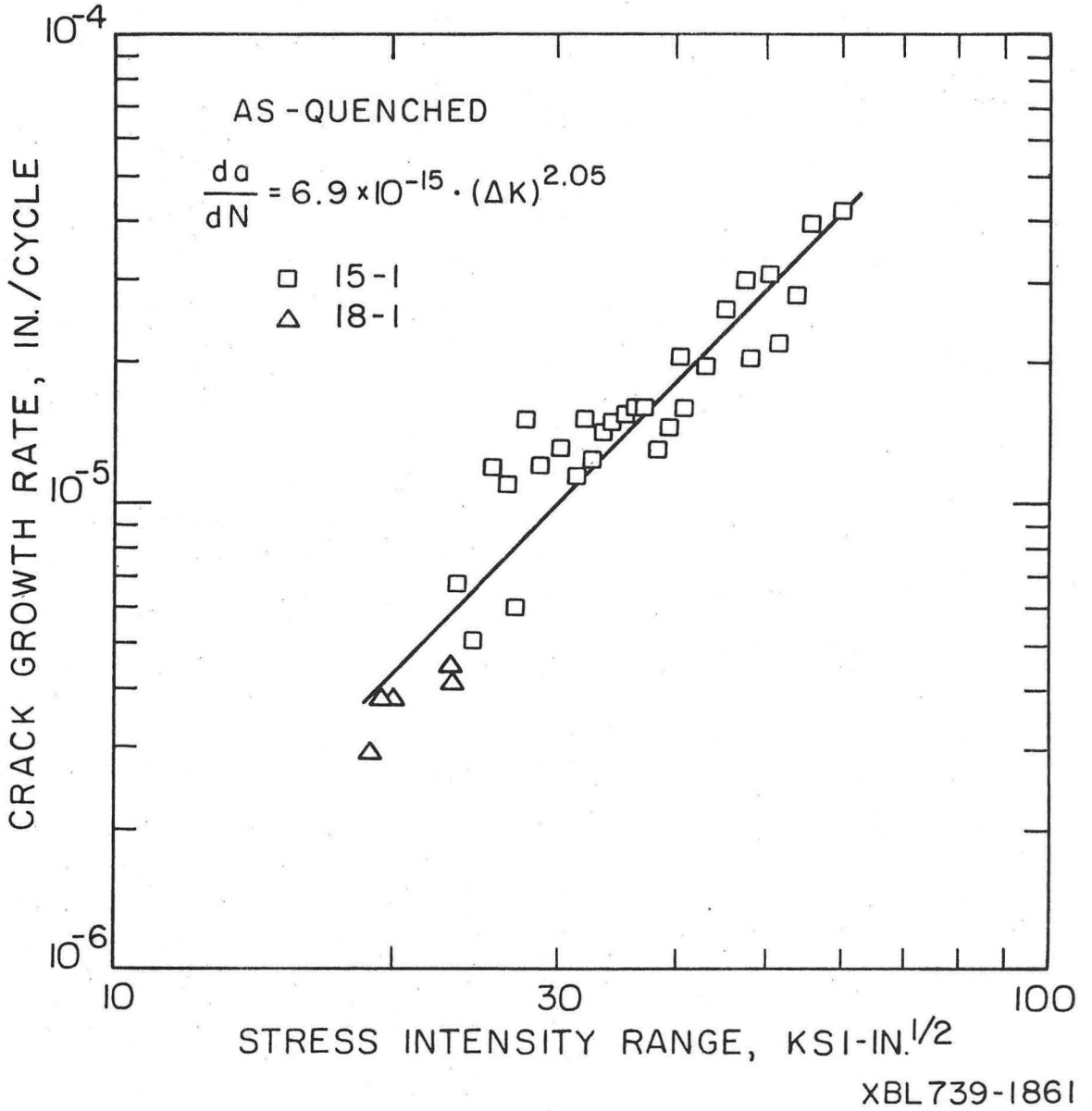
AS-QUENCHED
$\frac{da}{dN} = 6.9 \times 10^{-15} \cdot (\Delta K)^{2.05}$
15-1
18-1
10^{-4}
10^{-5}
10^{-6}
CRACK GROWTH RATE, IN./CYCLE
10
30
100
STRESS INTENSITY RANGE, KSI-IN.$^{1/2}$
XBL739-1861

Fig. 17

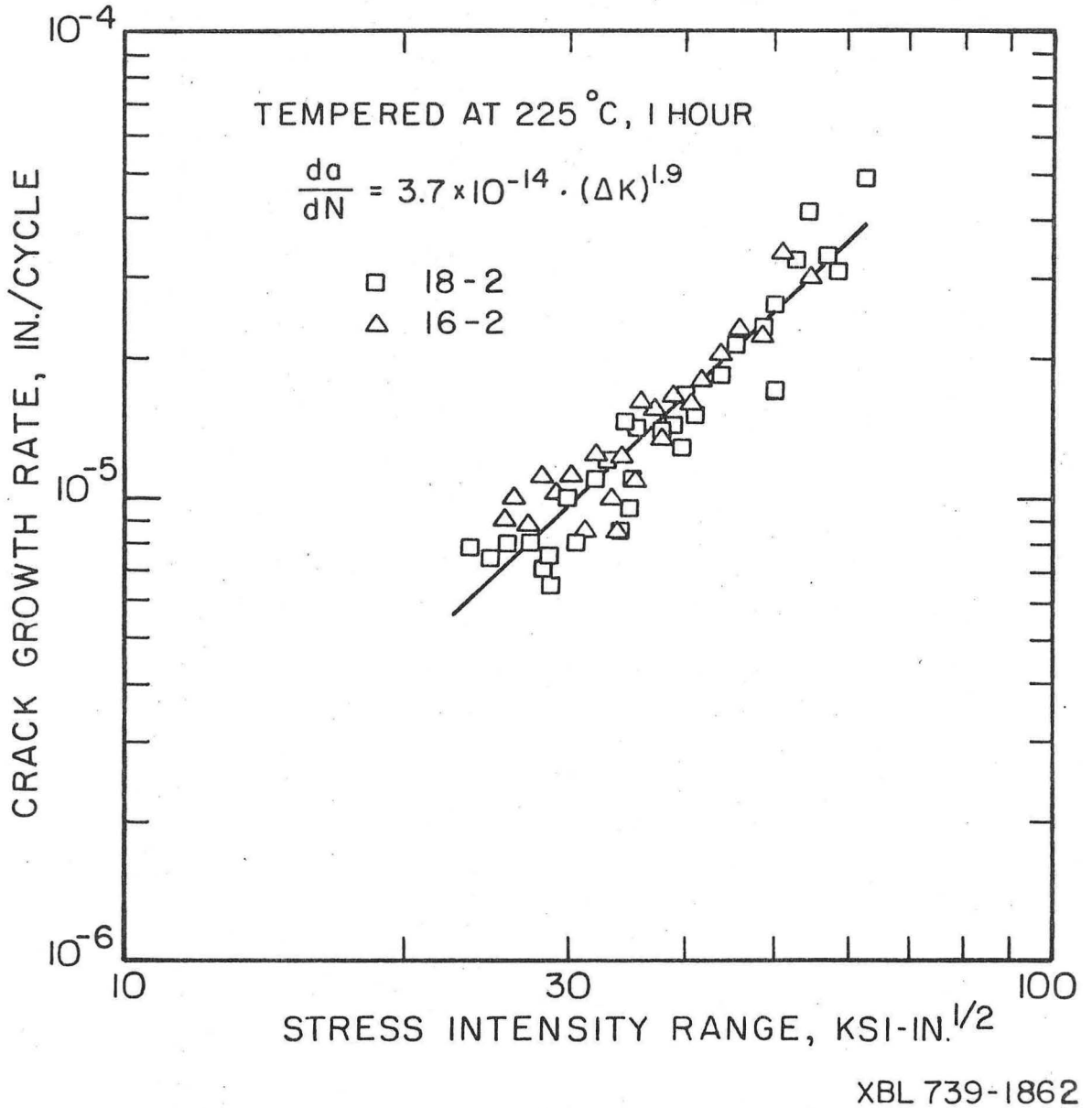
TEMPERED AT 225 °C, 1 HOUR
da/dN = 3.7 x 10^-14 · (ΔK)^1.9
18-2
16-2
CRACK GROWTH RATE, IN./CYCLE
10^-4
10^-5
10^-6
10
30
100
STRESS INTENSITY RANGE, KSI-IN.^1/2
XBL 739-1862

Fig. 18

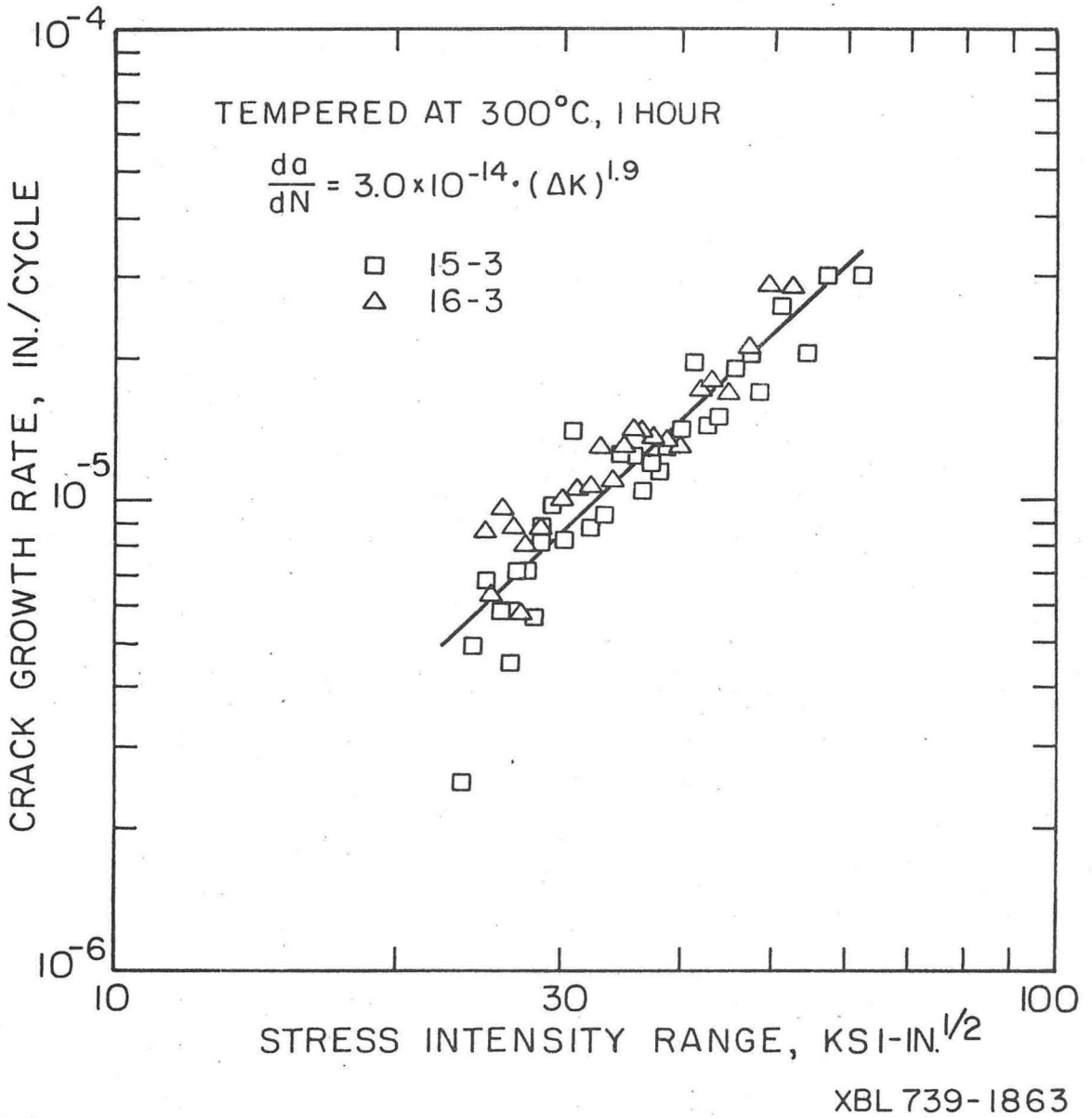
TEMPERED AT 300°C, 1 HOUR
$\frac{da}{dN} = 3.0 \times 10^{-14} \cdot (\Delta K)^{1.9}$
15-3
16-3
CRACK GROWTH RATE, IN./CYCLE
10^{-4}
10^{-5}
10^{-6}
10
30
100
STRESS INTENSITY RANGE, KSI-IN.$^{1/2}$
XBL 739-1863

Fig. 19

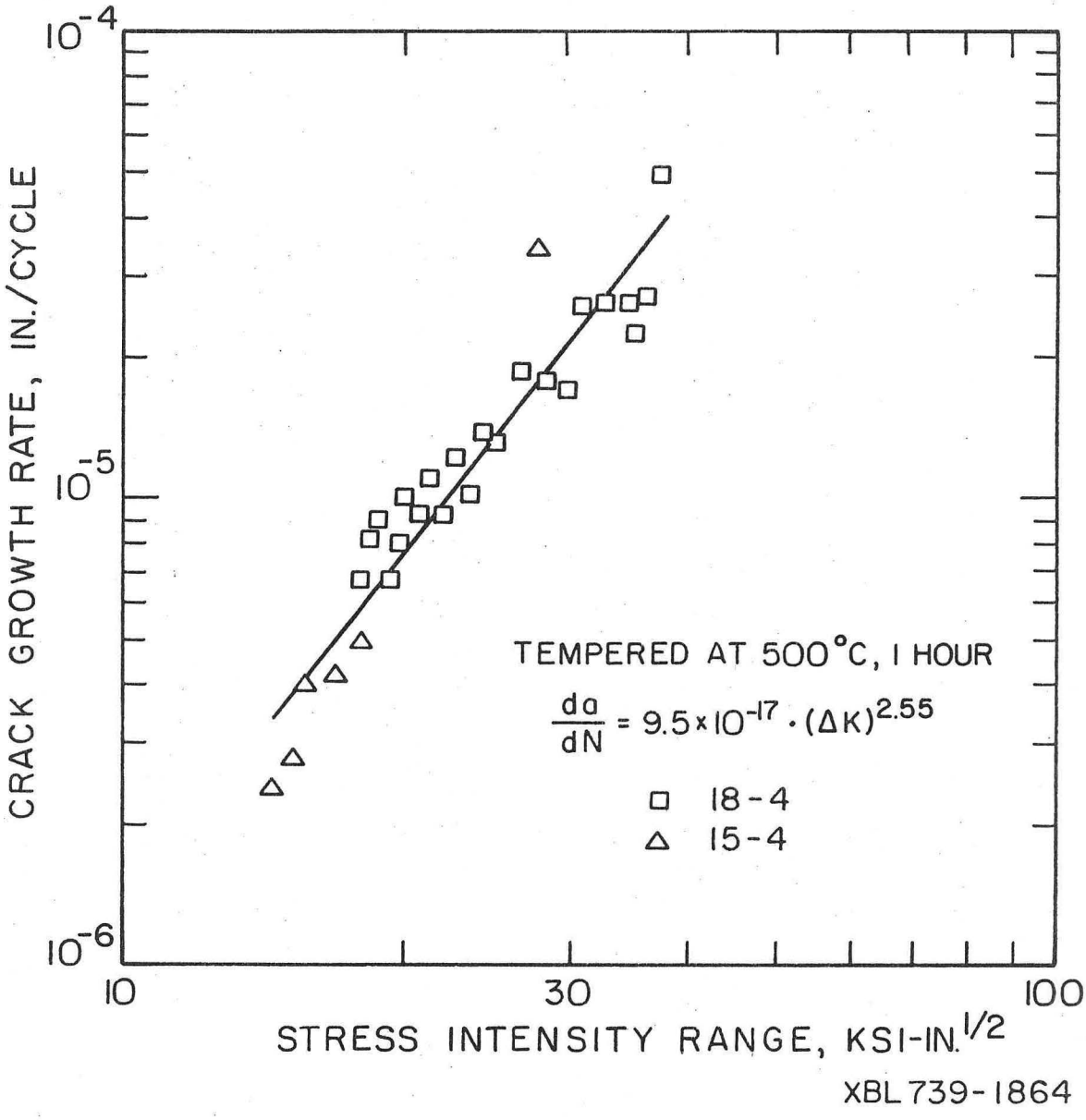
10^{-4}
10^{-5}
10^{-6}
CRACK GROWTH RATE, IN./CYCLE
10
30
100
STRESS INTENSITY RANGE, KSI-IN.$^{1/2}$
TEMPERED AT 500°C, 1 HOUR
$\frac{da}{dN} = 9.5 \times 10^{-17} \cdot (\Delta K)^{2.55}$
18-4
15-4
XBL 739-1864

Fig. 20

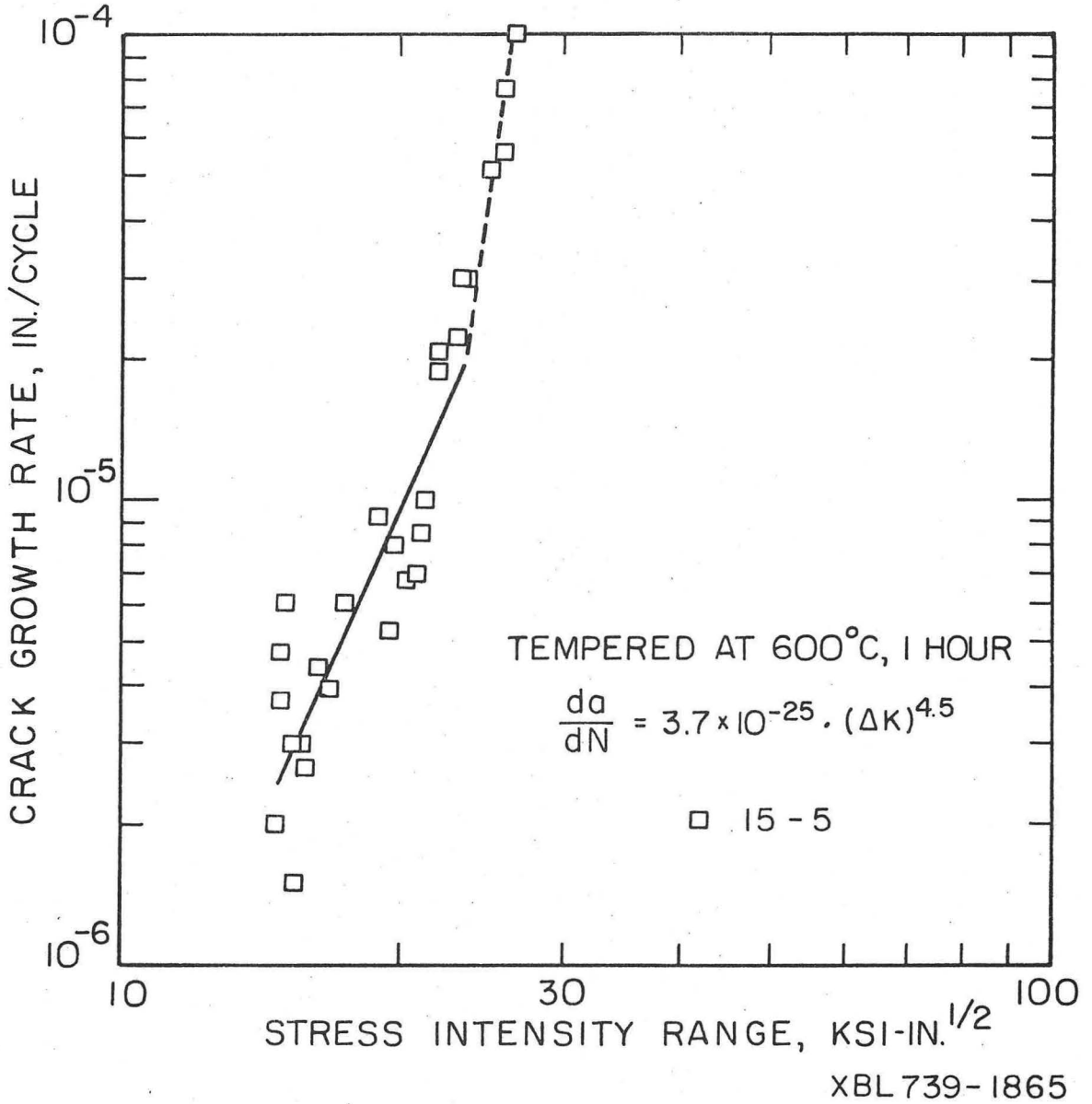
10^{-4}
10^{-5}
10^{-6}
CRACK GROWTH RATE, IN./CYCLE
TEMPERED AT 600°C, 1 HOUR
$\frac{da}{dN} = 3.7 \times 10^{-25} \cdot (\Delta K)^{4.5}$
15 - 5
10
30
100
STRESS INTENSITY RANGE, KSI-IN.$^{1/2}$
XBL 739-1865

Fig. 21

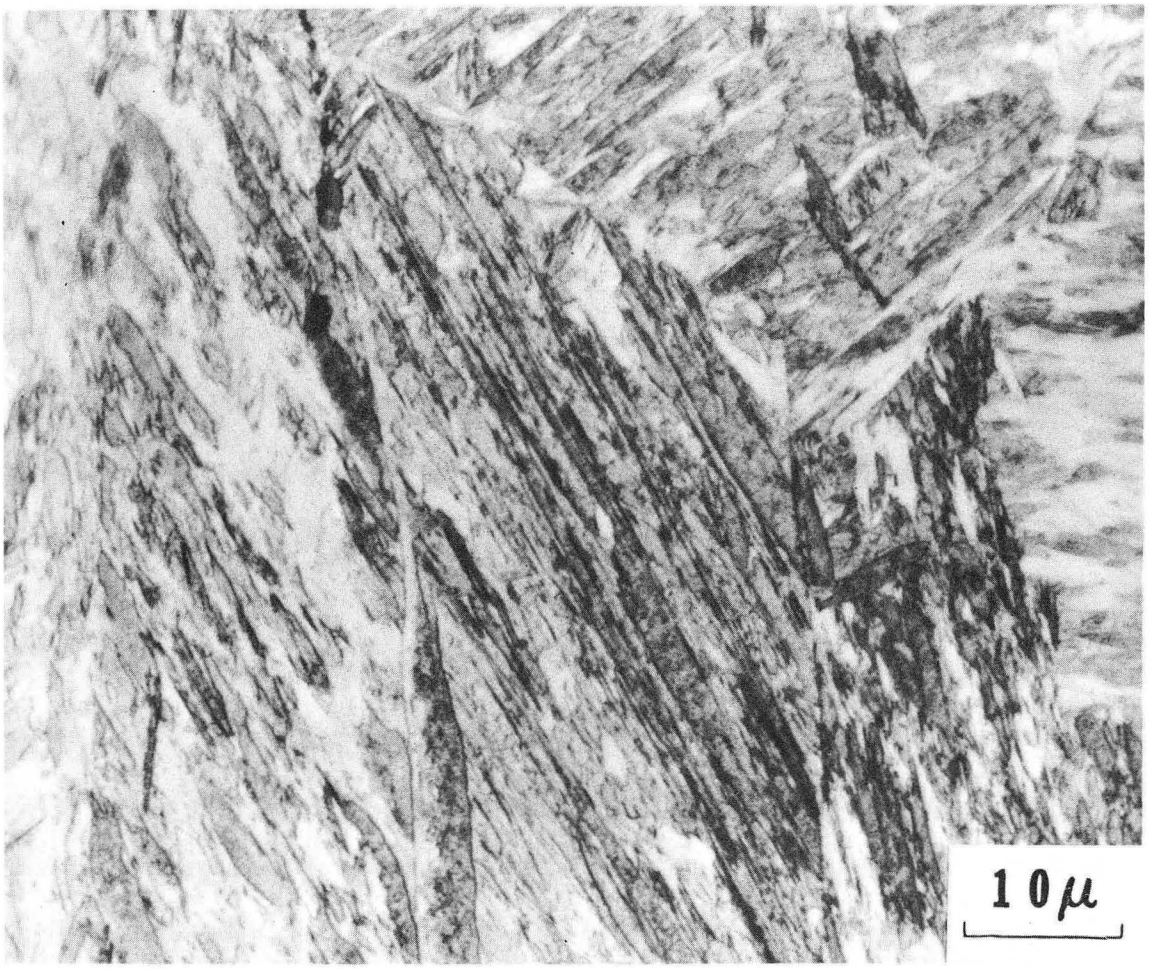

XBB 739-5584

Fig. 22

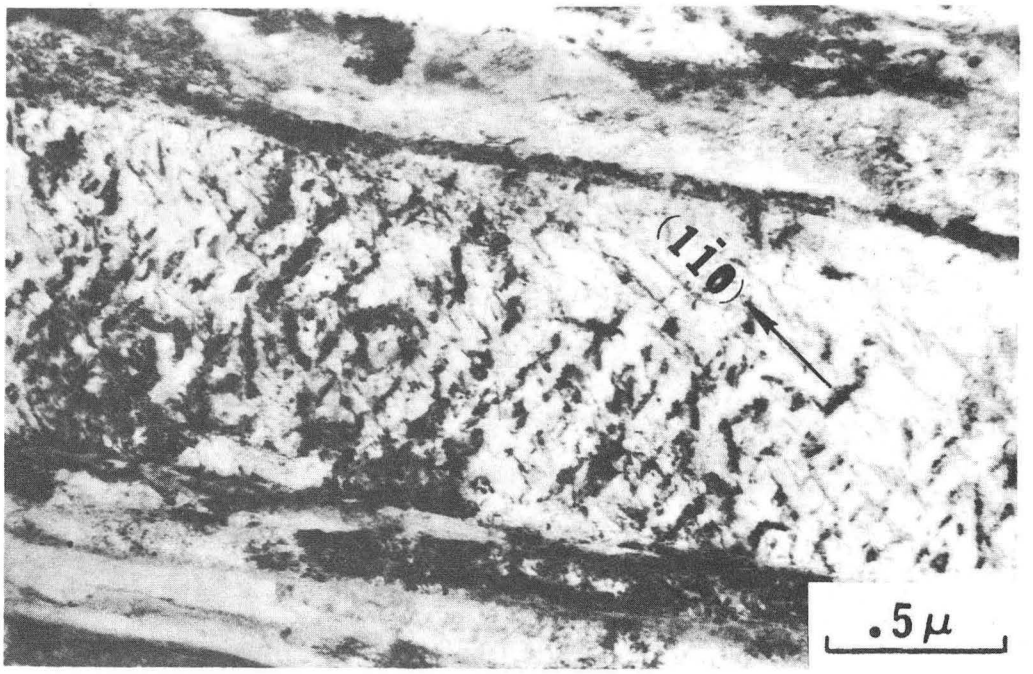

a

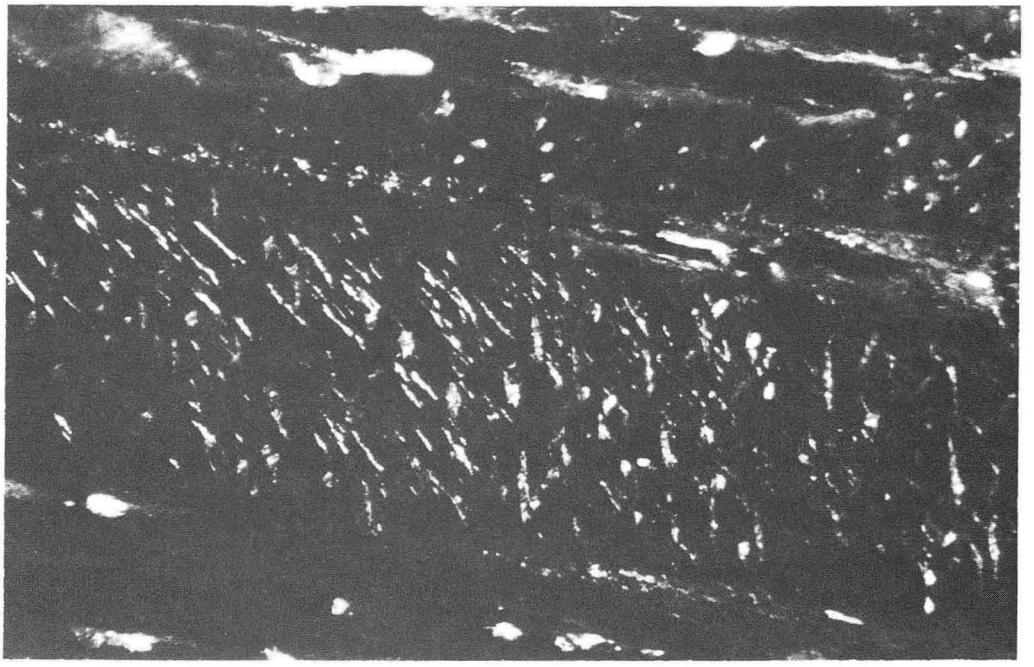

b XBB 7111-5567

Fig. 23

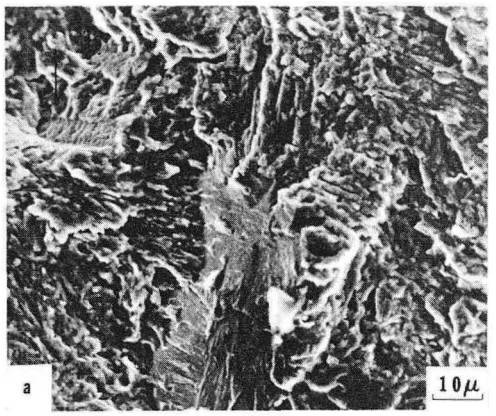

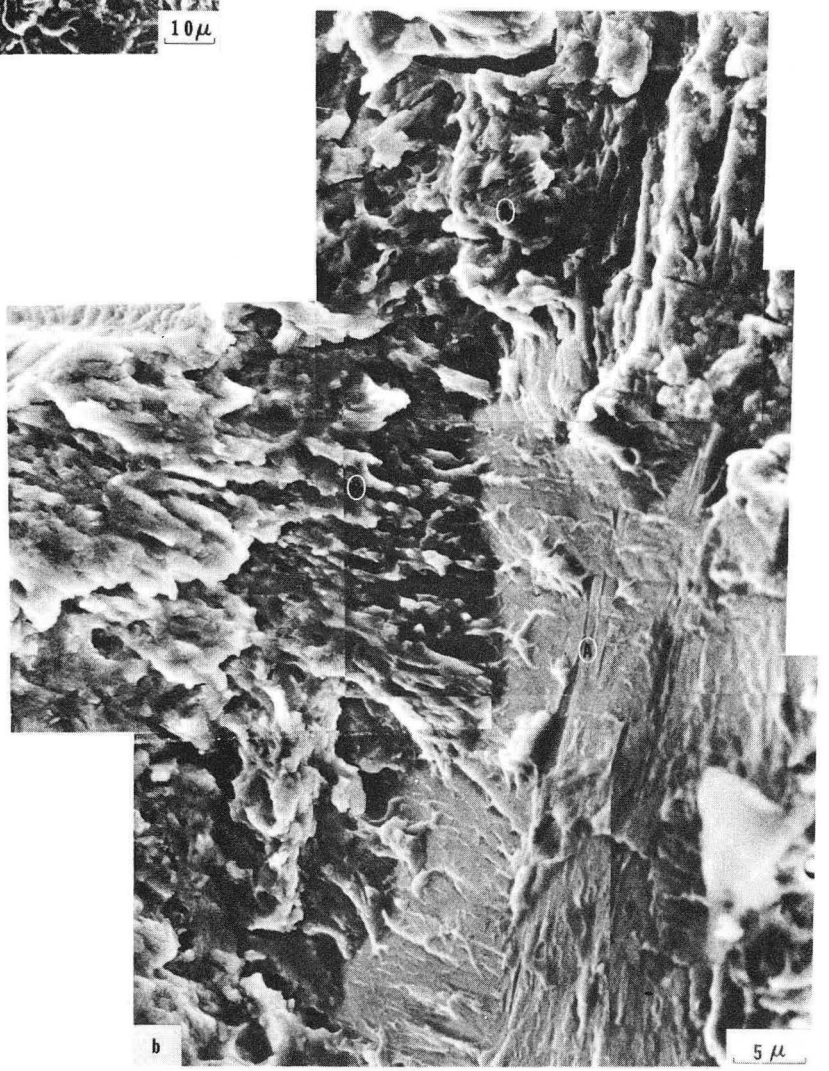

XBB 739-5579

Fig. 24

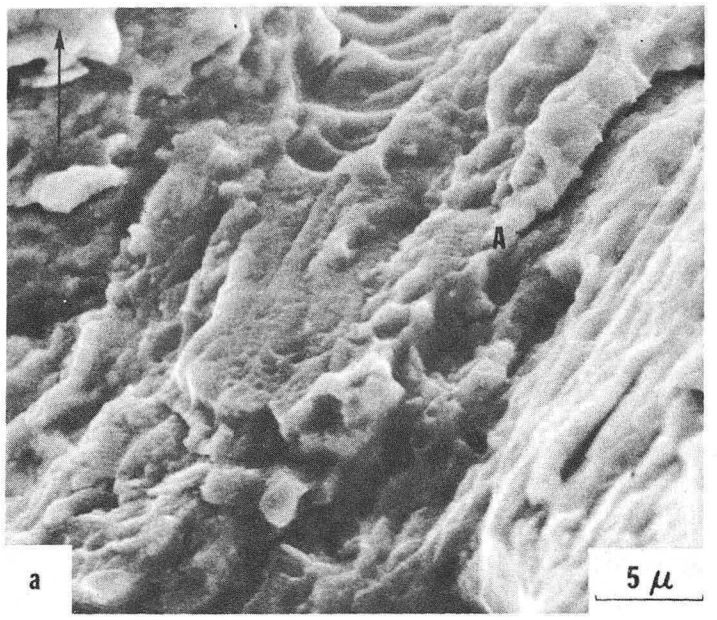

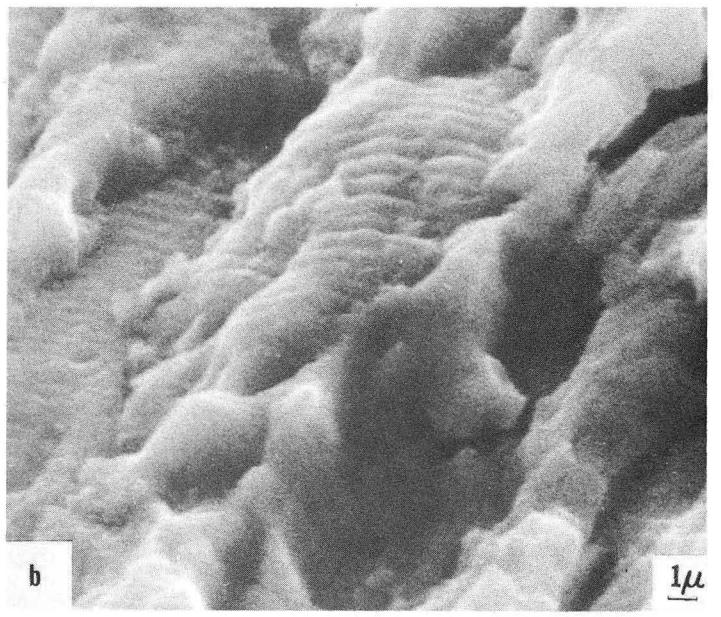

XBB 739-5581

Fig. 25

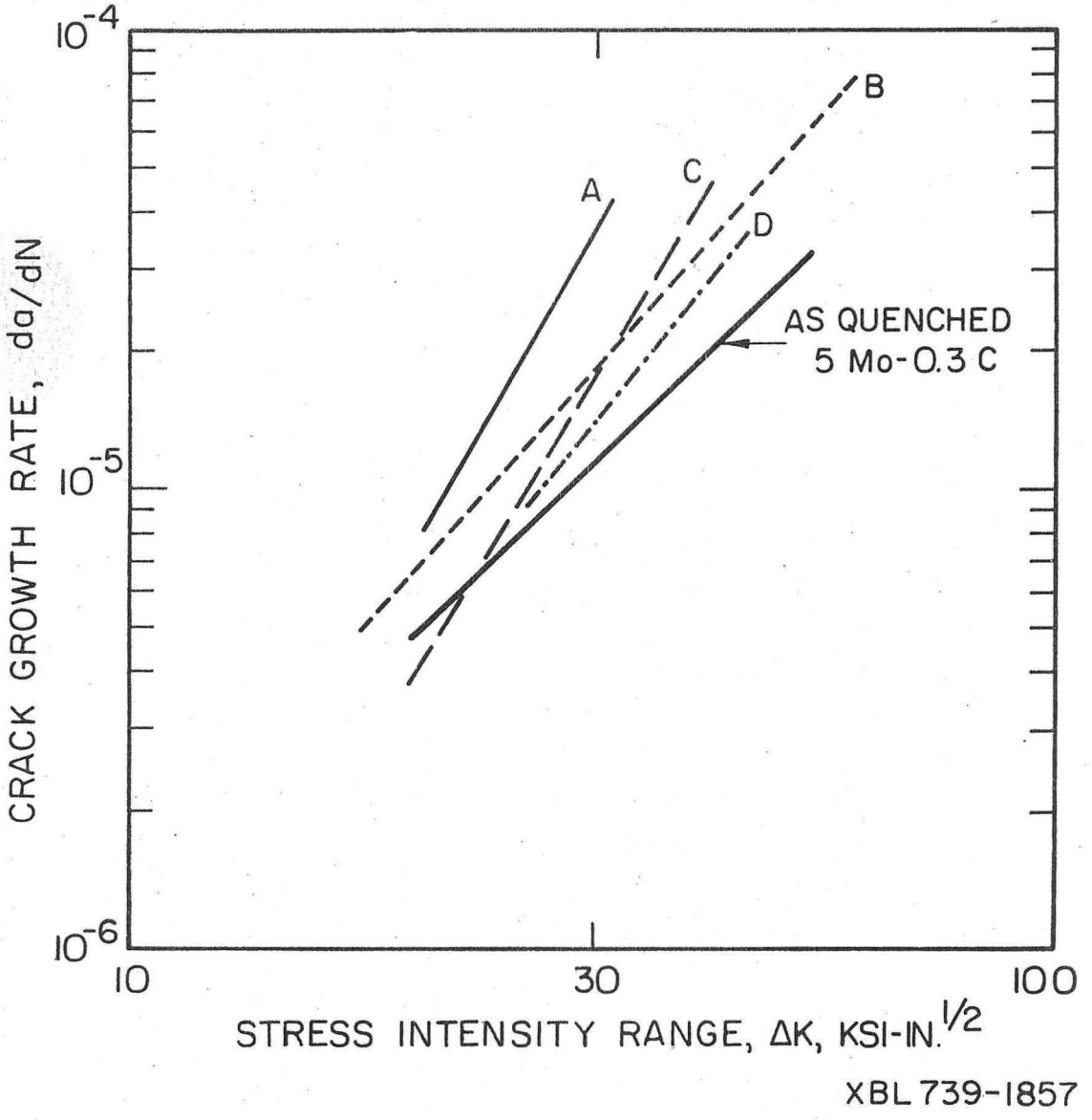
10^{-4}
10^{-5}
10^{-6}
CRACK GROWTH RATE, da/dN
A
B
C
D
AS QUENCHED
5 Mo-0.3 C
10
30
100
STRESS INTENSITY RANGE, ΔK, KSI-IN.$^{1/2}$
XBL 739-1857

Fig. 26

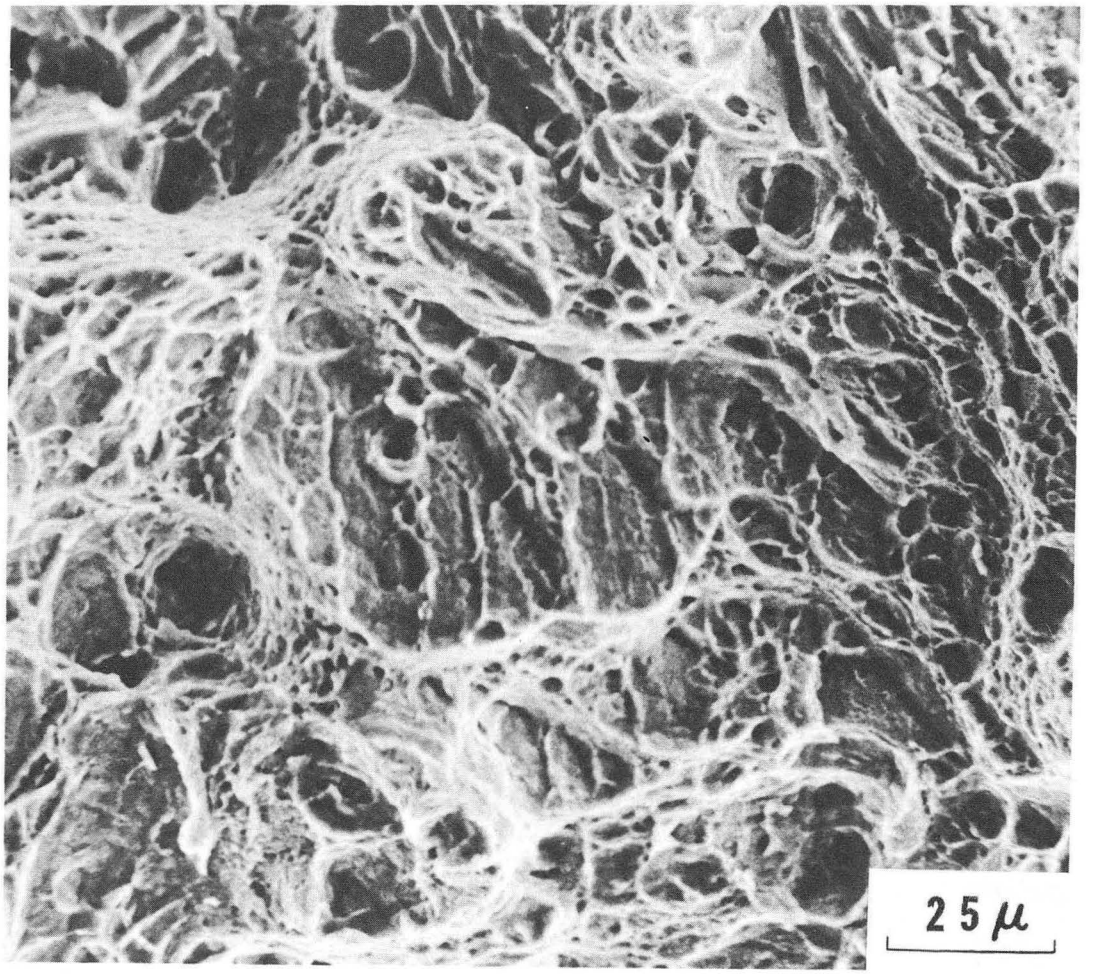

XBB 739-5587

Fig. 27

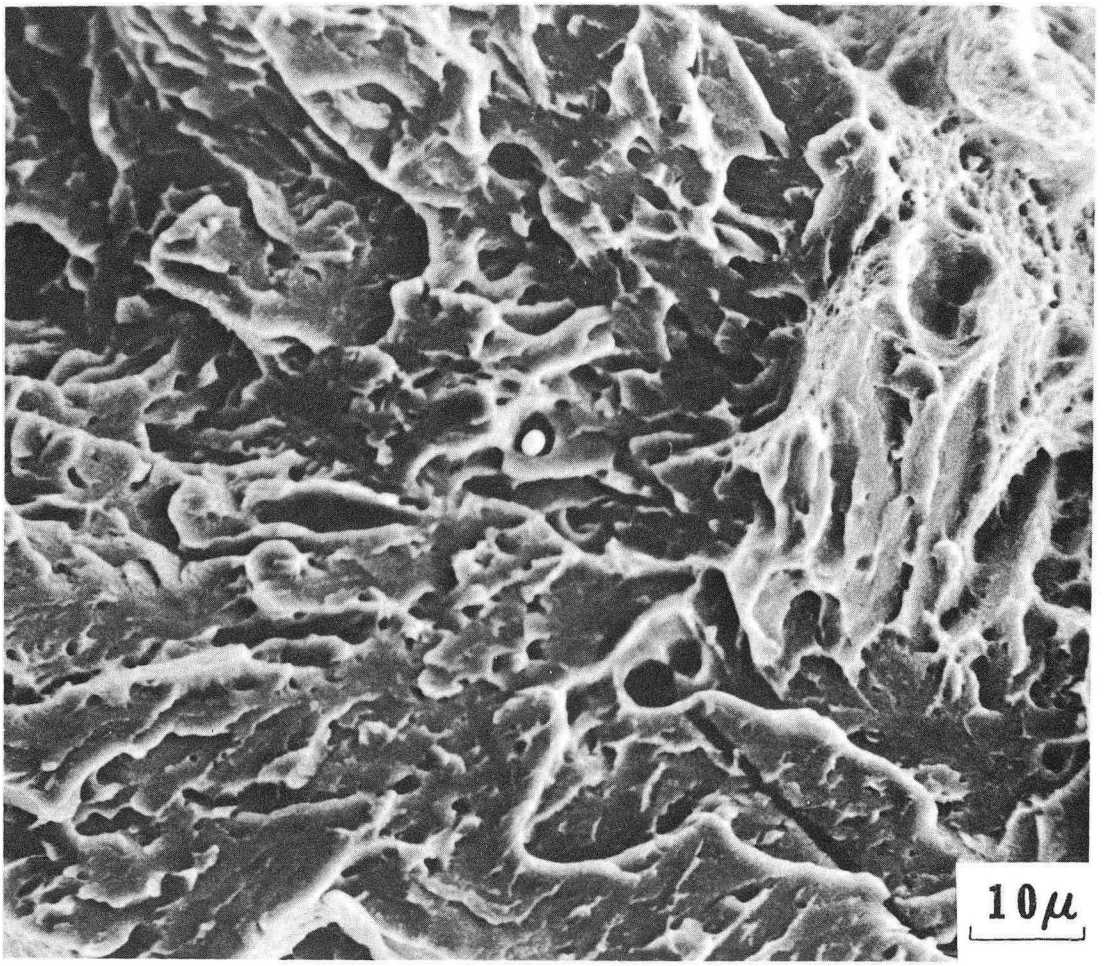

XBB 739-5586

Fig. 28

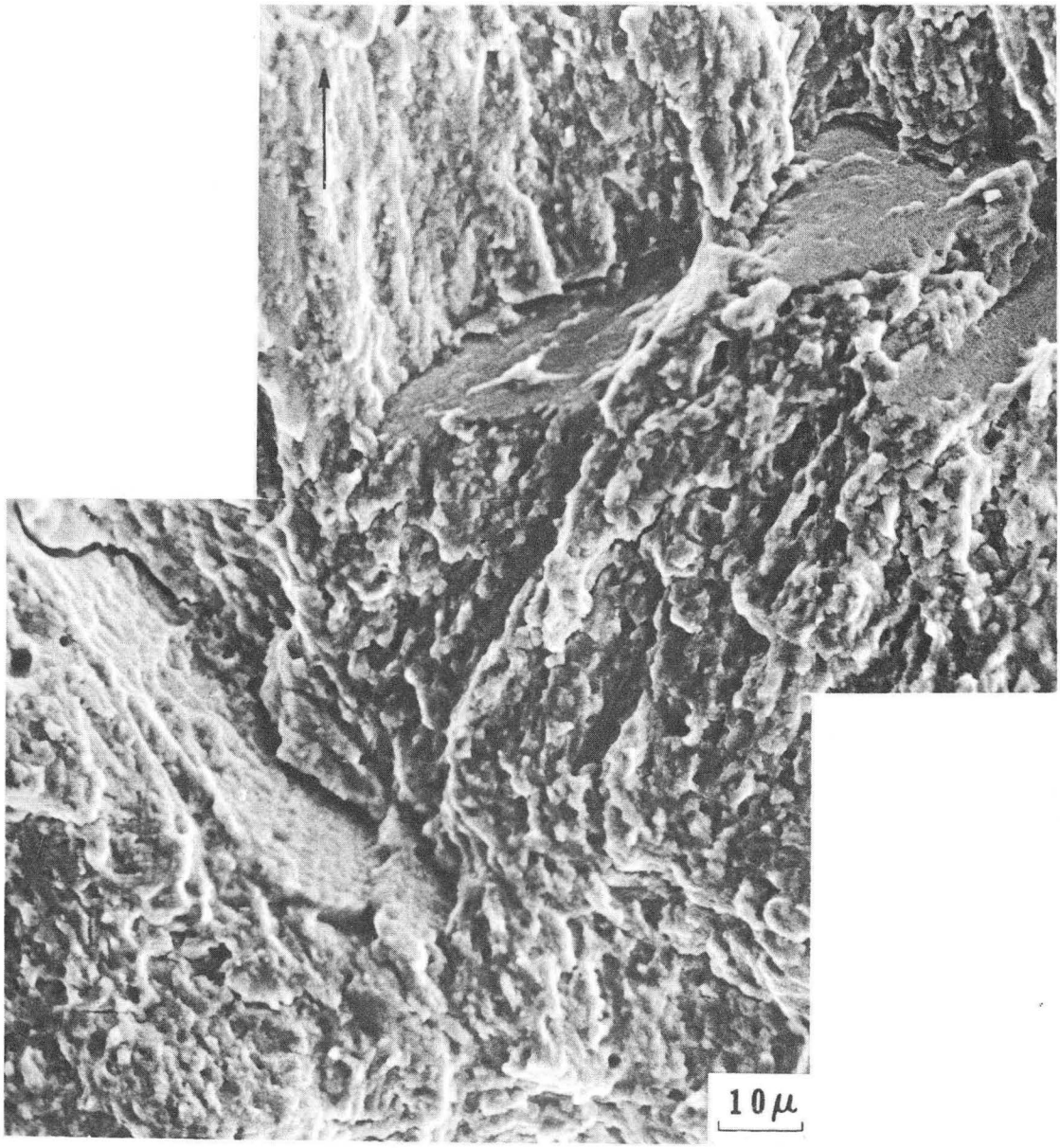

XBB 739-5580

Fig. 29

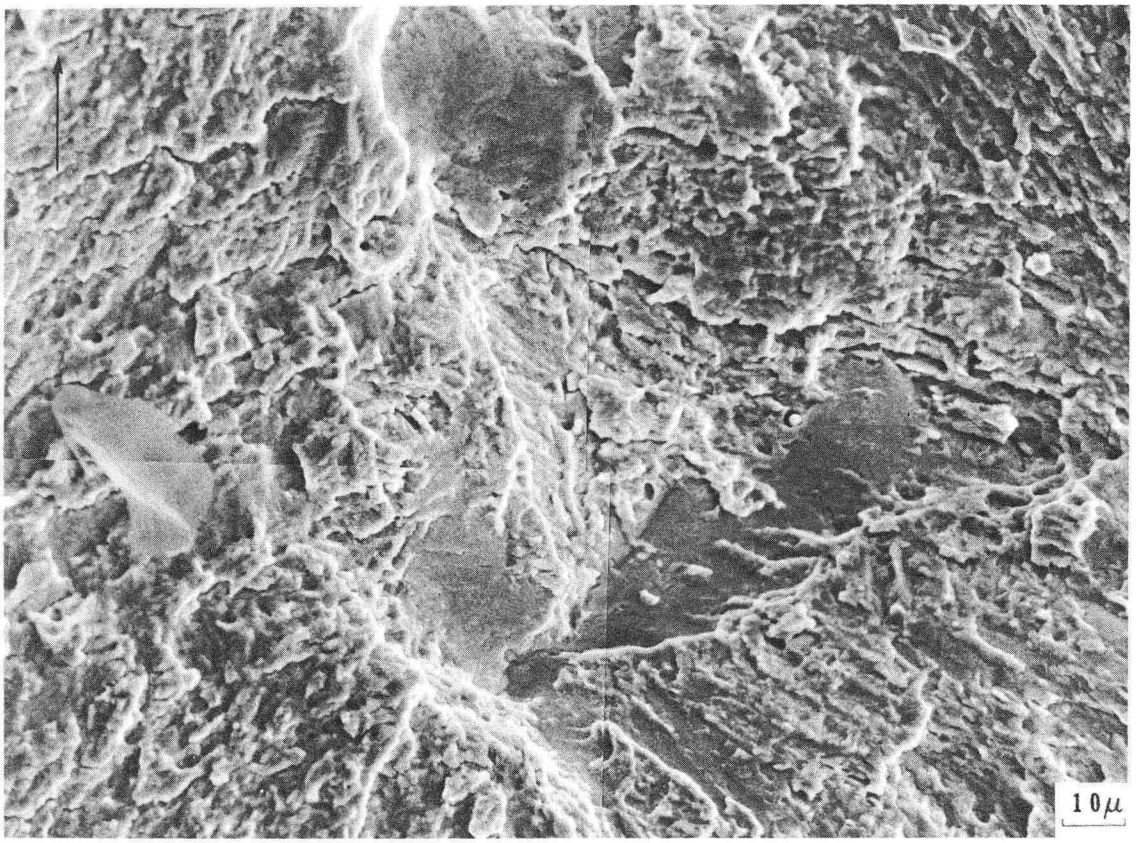

XBB 739-5582

Fig. 30

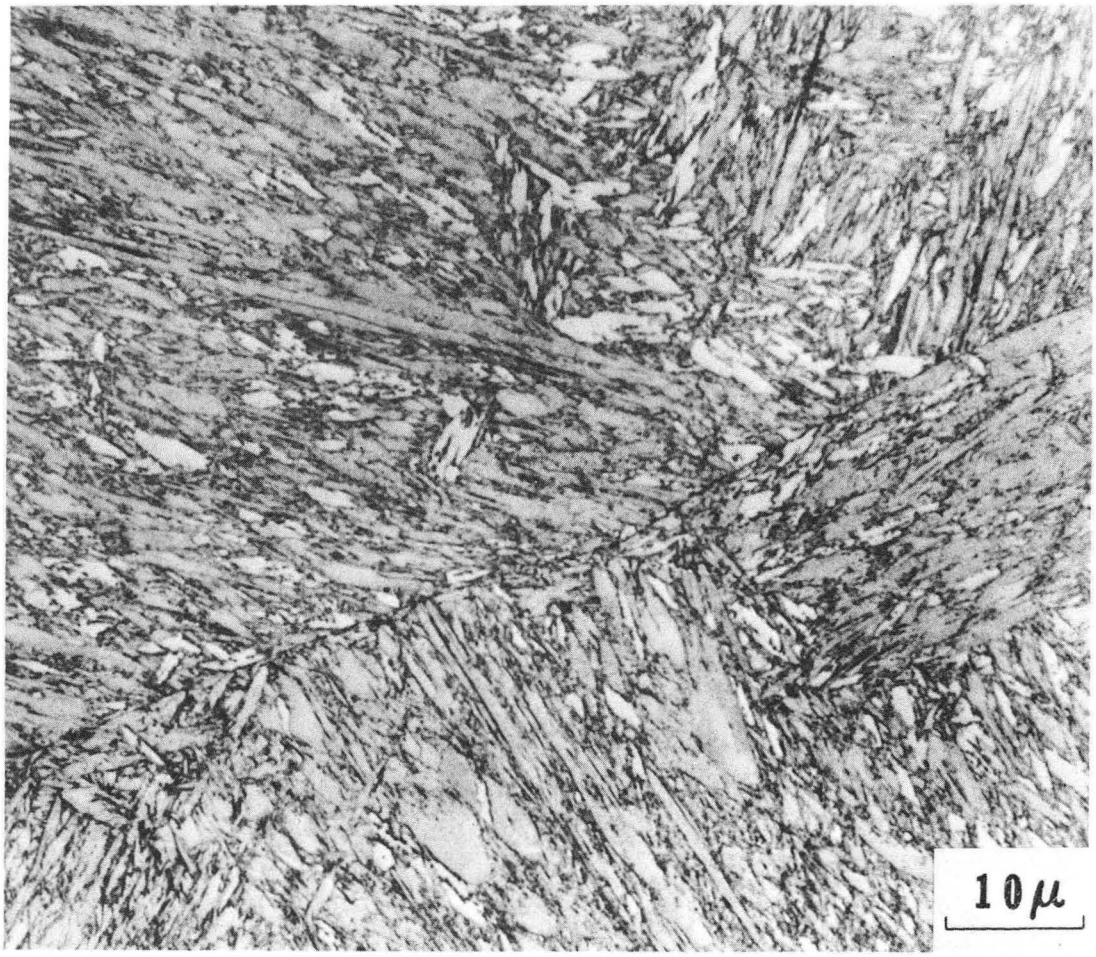

XBB 739-5585

Fig. 31

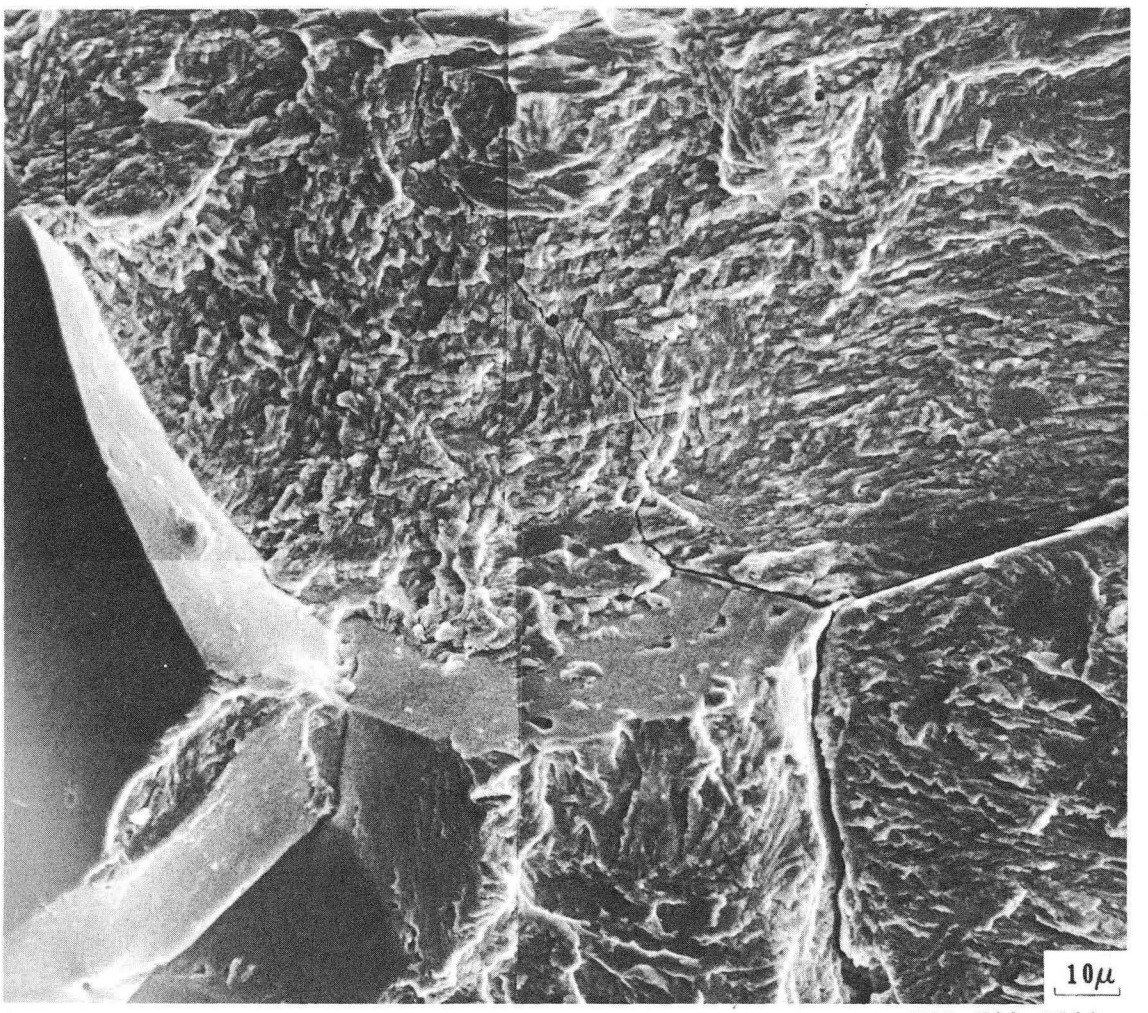

XBB 739-5583

Fig. 32

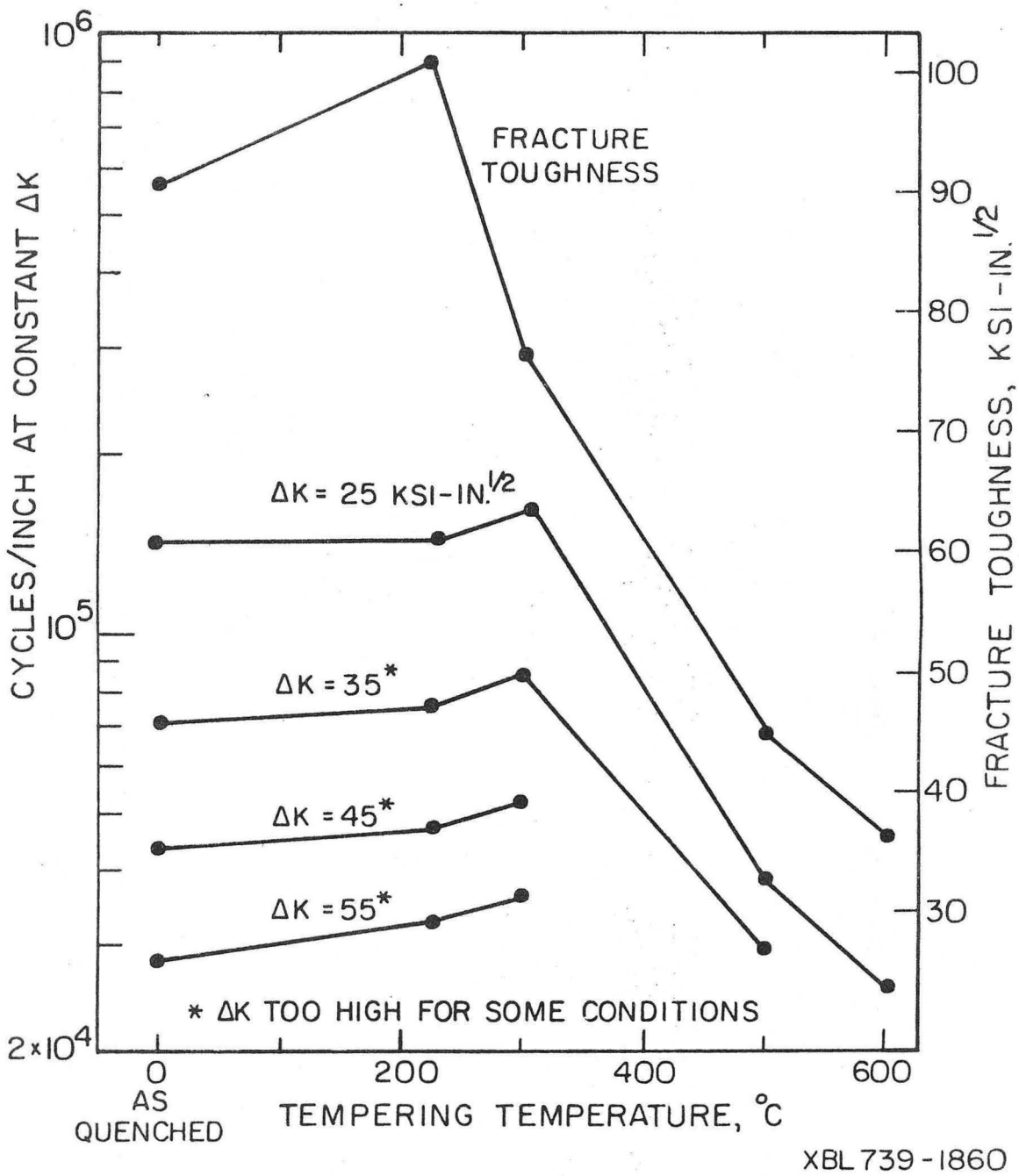
CYCLES/INCH AT CONSTANT ΔK
FRACTURE TOUGHNESS, KSI-IN.1/2
FRACTURE TOUGHNESS
ΔK = 25 KSI-IN.1/2
ΔK = 35*
ΔK = 45*
ΔK = 55*
* ΔK TOO HIGH FOR SOME CONDITIONS
10^6
10^5
2×10^4
100
90
80
70
60
50
40
30
0
AS QUENCHED
200
400
600
TEMPERING TEMPERATURE, °C
XBL 739-1860

Fig. 33

LEGAL NOTICE

This report was prepared as an account of work sponsored by the United States Government. Neither the United States nor the United States Atomic Energy Commission, nor any of their employees, nor any of their contractors, subcontractors, or their employees, makes any warranty, express or implied, or assumes any legal liability or responsibility for the accuracy, completeness or usefulness of any information, apparatus, product or process disclosed, or represents that its use would not infringe privately owned rights.

TECHNICAL INFORMATION DIVISION
LAWRENCE BERKELEY LABORATORY
UNIVERSITY OF CALIFORNIA
BERKELEY, CALIFORNIA 94720